Article

Cell Systems

The *Smarcal1-Usp37* locus modulates glycogen aggregation in astrocytes of the aged hippocampus

Graphical abstract

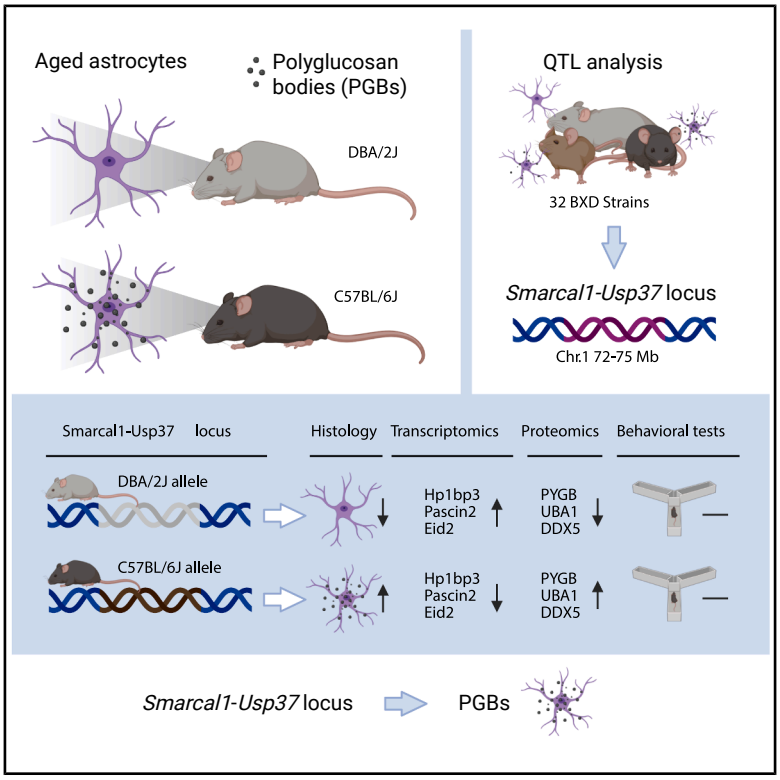

Highlights

- Aged hippocampal astrocytes with dysregulated autophagy accumulate polyglucosan bodies
- The *Smarcal1-Usp37* locus modulates strain-dependent variation in polyglucosan burden
- Age-related polyglucosan body build-up does not correlate with cognitive performance

Authors

Alicia Gómez-Pascual, Dow M. Glikman, Hui Xin Ng, ..., Rupert W. Overall, Robert W. Williams, Dennis E.M. de Bakker

Correspondence

labwilliams@gmail.com (R.W.W.), dennis.debakker@leibniz-fli.de (D.E.M.d.B.)

In brief

Gómez-Pascual et al. identified that in the aged murine hippocampus, astrocytes with impaired autophagy accumulate polyglucosan bodies. Their burden, which is modulated by the *Smarcal1-Usp37* locus, varies across strains but shows no clear link to cognitive performance.

Gómez-Pascual et al., 2026, Cell Systems *17*, 101488
February 18, 2026
https://doi.org/10.1016/j.cels.2025.101488

CellPress

Cell Systems

CellPress
OPEN ACCESS

Article

The *Smarcal1-Usp37* locus modulates glycogen aggregation in astrocytes of the aged hippocampus

Alicia Gómez-Pascual,[1,16] Dow M. Glikman,[2,16] Hui Xin Ng,[3,16] James E. Tomkins,[4,16] Lu Lu,[5] Ying Xu,[6,7] David G. Ashbrook,[5] Catherine Kaczorowski,[8] Gerd Kempermann,[9] John Killmar,[5] Khyobeni Mozhui,[5,10] Oliver Ohlenschläger,[11] Rudolf Aebersold,[12] Donald K. Ingram,[13] Evan G. Williams,[14] Mathias Jucker,[6,7] Rupert W. Overall,[15] Robert W. Williams,[5,*] and Dennis E.M. de Bakker[11,17,*]

[1]Department of Information and Communications Engineering, University of Murcia, Murcia 30003, Spain
[2]Institute of Science and Technology Austria, Am Campus 1, Klosterneuburg 3400, Austria
[3]Department of Cognitive Science, University of California, San Diego, CA 92093-0515, USA
[4]Centre for Misfolding Diseases, Department of Chemistry, University of Cambridge, Cambridge CB21EW, UK
[5]Department of Genetics, Genomics and Informatics, University of Tennessee Health Center, Memphis, TN, USA
[6]Department of Cellular Neurology, Hertie-Institute for Clinical Brain Research, University of Tübingen, Tübingen 72076, Germany
[7]German Center for Neurodegenerative Diseases (DZNE), Tübingen 72076, Germany
[8]Department of Neurology, University of Michigan, Ann Arbor, MI 48109, USA
[9]German Center for Neurodegenerative Diseases (DZNE), Dresden 01307, Germany
[10]Department of Preventive Medicine, College of Medicine, University of Tennessee Health Center, Memphis, TN 38163, USA
[11]Leibniz Institute on Aging – Fritz Lipmann Institute (FLI), Jena 07745, Germany
[12]Department of Biology, Institute of Molecular Systems Biology, ETH Zurich. Zurich 8049, Switzerland
[13]Pennington Biomedical Research Center, Louisiana State University, Baton Rouge, LA 70808-4124, USA
[14]Luxembourg Centre for Systems Biomedicine, University of Luxembourg, Belval 4362, Luxembourg
[15]Humboldt University of Berlin, Berlin 10099, Germany
[16]These authors contributed equally
[17]Lead contact
*Correspondence: labwilliams@gmail.com (R.W.W.), dennis.debakker@leibniz-fli.de (D.E.M.d.B.)
https://doi.org/10.1016/j.cels.2025.101488

SUMMARY

In aged humans and mice, hypobranched glycogen aggregates, known as polyglucosan bodies (PGBs), accumulate in hippocampal astrocytes. While PGBs are linked to cognitive decline in neurological diseases, they remain largely unstudied in the context of typical aging. We show that PGBs arise in autophagy-dysregulated astrocytes in the aged hippocampus, with substantial variation among 32 inbred BXD mouse strains. Genetic mapping through quantitative trait locus analysis identified a major locus (*Pgb1*) that modulates hippocampal PGB burden. Extensive transcriptomic and proteomic datasets were produced for the aged hippocampus of the BXD family to investigate the mechanism by which the *Pgb1* locus modulates PGB burden. We identified that *Pgb1* contains allelic *Smarcal1* and *Usp37* variants and influences PGB burden through *trans*-regulation of mRNA and protein expression levels, including abundance of glycogen-mobilizing factor PYGB. Furthermore, comprehensive phenome-wide association scans, transcriptomic analyses, and direct behavioral testing demonstrated that cognition remains intact despite age-related PGB burden. A record of this paper's transparent peer review process is included in the supplemental information.

INTRODUCTION

Polyglucosan bodies (PGBs) are formed by the aggregation of hypobranched glycogen molecules. Accumulation of PGBs is associated with neurodegenerative diseases, including adult PGB disease (APBD) and Lafora disease.[1] APBD is a rare neurogenetic disorder in which mutations in glycogen branching enzyme 1 (*GBE1*) reduce the efficiency of glycogen branching, leading to hypobranched glycogen molecules prone to aggregation.[2,3] These aberrant glycogen chains aggregate in neurons and astrocytes, which is associated with cellular dysfunction across the peripheral and central nervous systems.[4] As a result, APBD patients suffer severe peripheral neuropathy, muscle weakness, and dementia. In Lafora disease, caused by mutations in the epilepsy progressive myoclonus type 2 gene (*EPM2A*) and NHL repeat-containing E3 ubiquitin protein ligase 1 (*NHLRC1*), PGBs accumulate in many tissues, including the brain, skin, liver, heart, and skeletal muscle. Typically, this leads to ataxia and seizures in adolescence and the progressive development of severe dementia.[4–7]

In addition to their role in neurological diseases, PGBs also arise in the aging human brain under non-pathological

conditions, referred to as *corpora amylacea*.[4,8,9] Age-related glycogen aggregates, which share features with human *corpora amylacea* while exhibiting differences in size and conventional staining properties, also form in the hippocampus of the C57BL/6J mouse strain.[10,11] Due to these reported differences, we refer to the mouse glycogen aggregates by the categorical term "PGBs." In both humans and mice, these age-related PGBs are most prominent in astrocytes of the hippocampus but can also be found in other regions and cell types of the aged brain.[4,10–12]

The astrocyte-specific accumulation of PGBs is likely due to the central role these glial cells play in glycogen homeostasis of the brain.[13] Astrocytes are a heterogeneous cell population with distinct specialized functions, and characterization of these functionalities is an ongoing process.[14] For example, a subset of hippocampal astrocytes has recently been identified to show age-related autophagy dysregulation, leading to severely inflated autophagosomes. Although direct relevance to cognitive function was not shown, these autophagy-dysregulated astrocytes (APDAs) had detrimental effects on the number of synapses in adjacent neurons.[15] Furthermore, astrocytic dysfunction could directly affect the age-related decline of hippocampal function, considering that hippocampal astrocytes play an active role in memory consolidation and the location-specific encoding of the reward system.[16–20]

Here, we investigate the genetic architecture underlying misfolded glycogen aggregates in the aged hippocampus by analyzing the age-related occurrence of PGBs in 32 different BXD (C57BL/6J crossed with DBA/2J) recombinant inbred mouse strains. One of the primary uses of the BXD family is to map genetic regions, also called quantitative trait loci (QTLs), which influence phenotypic variation of a complex trait.[21,22] Utilizing the BXD cohort and QTL mapping, together with behavioral and hippocampal transcriptomic and proteomic datasets, we identify a genetic locus modulating hippocampal PGB burden and evaluate the pathophysiological significance of these age-related glycogen aggregates.

RESULTS

PGBs accumulate in autophagy-dysregulated astrocytes

To determine the cell type in which PGBs accumulate, we validated the occurrence of PGBs in the hippocampus of 18–24-month-old C57BL/6J male and female mice using antibodies targeting LBP110.[10] While periodic acid-Schiff (PAS) staining is a reliable method for detecting PGBs in paraffin sections, its application to thicker, fixed frozen sections presents substantial challenges.[10] However, fixed frozen samples were available for quantifying PGBs in BXD recombinant strains. Therefore, we employed the LBP110 antibody for PGB visualization in this study, as it has been demonstrated to be a reliable method.[10] PGB burden was most pronounced in the CA1 and CA2 regions of the hippocampus but was also evident in all other hippocampal subregions, including the dentate gyrus (Figures 1A and 1B). Double labeling with the astrocytic marker glial fibrillary acidic protein (GFAP) validated that PGBs are mainly localized to astrocytes and that a single astrocyte can contain a cluster of PGBs (Figure 1C), which is in accordance with previous literature.[9,10] Considering that the accumulation of glycogen might be linked to compromised autophagy,[23,24] we assessed whether PGBs arise in the recently defined APDAs.[15] Therefore, consecutive sections were stained with APDA marker Scrapie-responsive gene 1 (SCRG1) and autophagosome marker Sequestosome-1 (SQSTM1), which both resulted in a staining pattern reminiscent of LBP110 (Figures 1D and 1E). Indeed, fluorescent co-labeling of LBP110 and SQSTM1 showed a strong co-localization in the hippocampus (Figures 1F–1H), indicating that hippocampal PGBs arise specifically in APDAs.

Variation in hippocampal PGB burden maps to a gene-rich locus on chr 1

PGBs accumulate in the hippocampus of aged C57BL/6J (B6) but not DBA/2J (D2) mice.[10] To investigate whether this heterogeneity extends to the BXD strains, we quantified the number of PGB clusters in the hippocampus of 142 aged females (16–18 months old) sampled from 32 BXD strains and both parental strains, B6 and D2. The average number of PGB clusters, with a single cluster likely representing a single astrocyte, was determined from an average of four animals per strain (Table S1). Average PGB cluster counts varied over 400-fold among BXD strains, with a variation between 1.5 and 646 clusters per hippocampus (Figure 2A) (GeneNetwork dataset: BXD_10685). Extraordinarily high PGB burden was observed in B6 and BXD20 strains, while PGBs were nearly undetectable in D2 and BXD32 strains (Figures 2A–2E). The variation of PGB burden between the inbred BXD strains allowed us to correlate PGB burden with several layers of information available for these strains, including their fully sequenced genomes (Figure 2F). We analyzed which genetic loci contribute to differences in PGB burden, which was mapped using sequence-based markers and a linear mixed model regression (GEMMA), which corrects for kinship.[25,26] The PGB cluster numbers among strains were strongly skewed, and values were therefore $\log_{10}$ transformed prior to mapping (Figure S1) (GeneNetwork dataset: BXD_10686). The highest association was found on chromosome 1 (chr 1) at 72.5 Mb ($-\log p$ 4.9, GRCm38 mm10 assembly), with a 1.5 $-\log p$ confidence interval (CI) that ranged from 72.0 to 75.0 Mb (Figures 3A–3C and S2). Approximately 25% of the variance in PGB burden can be explained by this locus ($r = -0.51$, $p = 2.244 \times 10^{-3}$, $n = 34$ strains), hereafter referred to as the *Pgb1* locus (Figure 3D).

Candidate analysis identifies *Smarcal1* and *Usp37* as potential effectors of PGB burden

The *Pgb1* locus includes 94 potential coding regions, of which 47 encode validated transcripts (42 protein coding, four microRNAs, and one long non-coding RNA; Figure 4A). To define allele variants most likely to modulate PGB density from within the *Pgb1* locus, we accumulated available data for each of the 42 protein-coding genes (Table S2) and used specific selection criteria (Figure 4A).[27–30]

To begin, only protein-coding genes with a PGB burden linkage of $-\log p \geq 3$ were considered, resulting in 36 genes. Variant gene candidates could influence PGB density via two

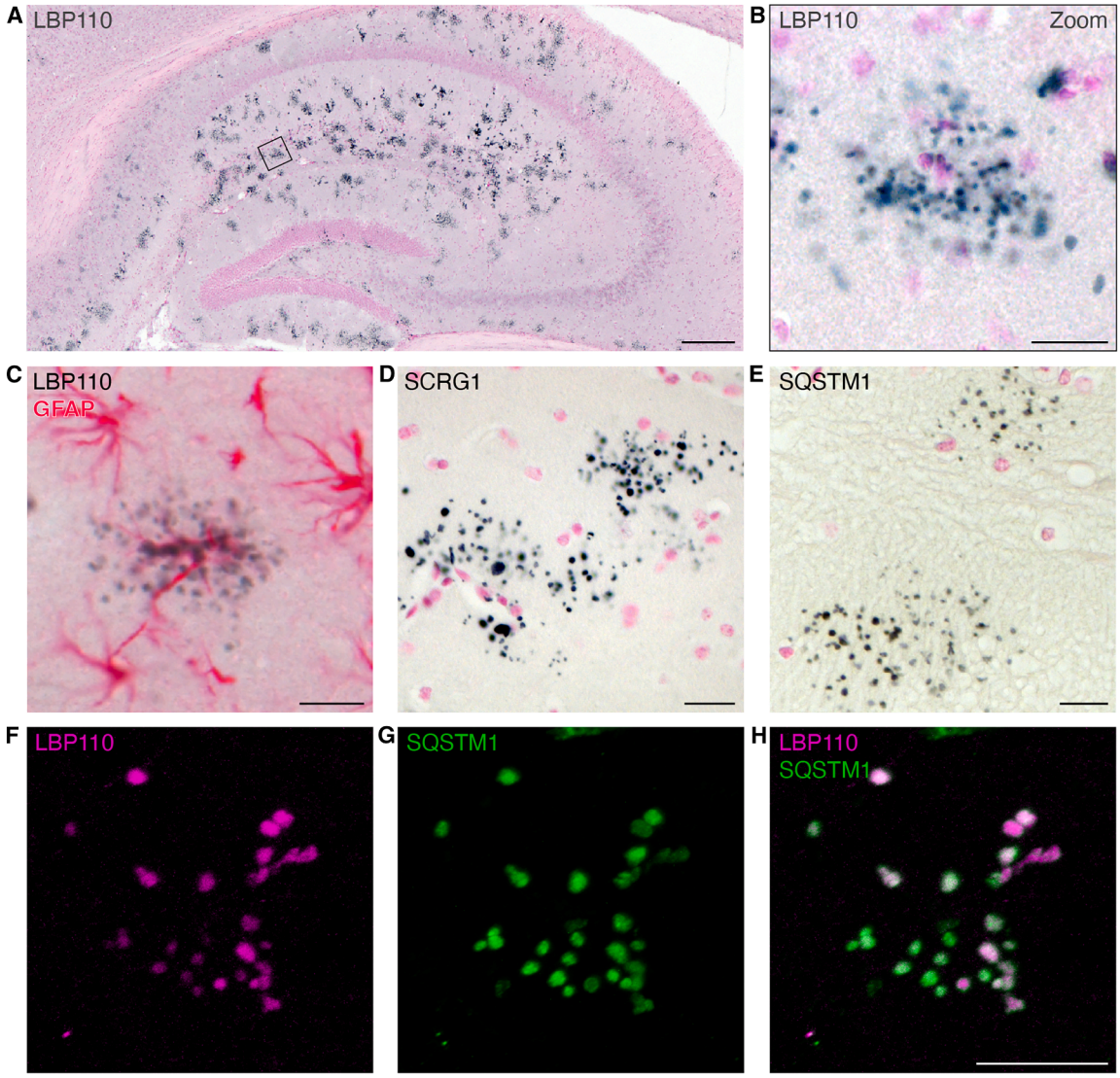

Figure 1. PGBs accumulate in the aging hippocampus

(A and B) The hippocampus of an 18-month-old female, stained with an anti-LBP110 antibody targeting PGBs. Scale bars represent 200 μm (A) or 20 μm (B).

(C) Antibody staining of astrocyte marker GFAP (magenta) and LBP110 (black), which binds PGBs.

(D) Antibody staining against SCRG1, a marker of APDAs.

(E) Antibody staining against SQSTM1, an autophagosome marker.

(F–H) Fluorescent antibody staining against SQSTM1 and LBP110, obtained from the dentate gyrus of a 2-year-old male. Scale bars (C–H) represent 20 μm.

distinct mechanisms, either by altering expression levels or by modifying protein function. To identify genes that exhibit altered expression levels due to allele variations within our target locus (a *cis*-regulatory effect), we produced extensive hippocampal exon array data from 235 BXD animals (223–972 days old; GeneNetwork dataset: GN392; Table S3). Analysis of mRNA expression QTL (eQTL) was performed to identify the locus modulating expression level differences among BXD strains. Notably, we found that seven out of 36 candidate genes mapped as a *cis*-eQTL to the *Pgb1* locus ($-\log p \geq 1.5$), suggesting that sequence variation near the candidates (e.g., in promoters or enhancers) directly affects their expression level. We then selected those candidates that displayed a significant correlation ($p < 0.05$) between transcript expression levels and PGB burden and identified three candidates: SWI/SNF-related, matrix-associated, actin-dependent regulator of chromatin, subfamily A-like 1 (*Smarcal1*), Tensin-1 (*Tns1*), and Ubiquitin-specific Peptidase 37 (*Usp37*) (Figure 4B). *Smarcal1* and *Tns1* were negatively correlated with PGB burden—correlations of −0.73 and −0.52, respectively—indicating a potential protective role for these genes against PGB burden. By contrast, *Usp37* exhibited a positive correlation with PGB burden (r = 0.509), suggesting a potential role in enhancing PGB frequency. Taken together, this analysis led to the identification of three candidate genes that may impact PGB burden through changes in gene expression levels.

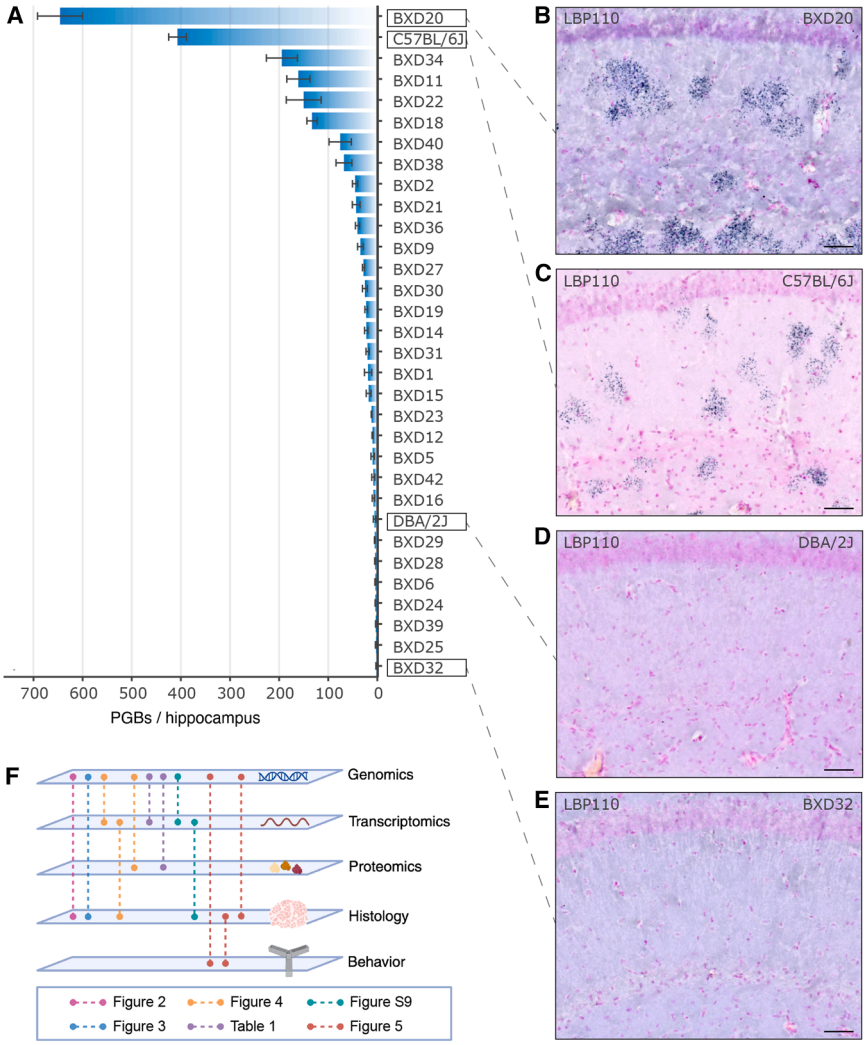

Figure 2. PGB accumulation in the hippocampus varies widely between BXD strains

(A) Average number of PGBs per hippocampus of 32 BXD strains, including parental strains C57BL/6J and DBA/2J. Genenetwork trait: BXD_10685. Error bars represent the standard error of the mean (SEM).

(B–E) Representative images of LBP110 staining in the hippocampus of the BXD20, C57BL/6J, DBA/2J, and BXD32 strains. Scale bars represent 50 μm.

(F) Graphical abstract of the strategy used to characterize the PGB phenotype.

Single-cell RNA sequencing indicates cell-type-specific activity of the *Pgb1* locus

We hypothesize that the *Pgb1* locus may directly affect astrocytes, as these are the cells accumulating PGBs (Figure 1C). To assess whether the *Pgb1* locus could indeed influence hippocampal astrocytes, we first examined whether high-priority candidate genes within the *Pgb1* locus (namely *Usp37* and *Smarcal1*) are expressed in hippocampal astrocytes. We utilized the Allen Brain Cell (ABC) Atlas, a comprehensive whole-brain single-cell RNA-sequencing dataset of ∼4 million cells.[32] These data revealed that in young mice (51–71 days old), both *Smarcal1* and *Usp37* are highly expressed in hippocampal astrocytes, as well as in other hippocampal cell types, including immune cells and glutamatergic and immature neurons (Figure S3).

Next, we validated the expression of *Smarcal1* and *Usp37* in astrocytes in an independent dataset containing both astrocytes and CA1/CA3 hippocampal neurons[33] and explored the influence of brain aging on cell-type-specific gene expression profiles (Figure S4). We found that, like young mice (2-month-old), aged mice (18-month-old) express *Smarcal1* and *Usp37* in multiple cell types of the brain. However, expression was notably enriched in astrocytes compared with CA1/CA3 neurons and showed an age-related increase (Figures S4A–S4D). This pattern was similarly observed in additional genes located at the *Pgb1* locus, including *Tns1* and *Bcs1l* (Figures S4E–S4H). Taken together, these findings support an astrocyte-specific relevance for *Pgb1* gene variants.

The transcription factor *Etv4* might underlie astrocyte-specific regulation of *Pgb1* locus genes

As *Usp37* and *Smarcal1* showed the highest expression in aged astrocytes relative to other hippocampal cell types, we next asked whether this astrocyte-specific enrichment could be driven by cell-type-specific transcription factors. To explore whether astrocyte-specific transcription factors contribute to this gene expression pattern, we investigated known regulators of *Usp37* and *Smarcal1*. First, we compiled a list of transcription factors predicted to

To identify candidates that may affect PGB burden via changes in protein function, we focused on candidates with at least one non-synonymous mutation between the *B* and *D* alleles. From eight candidate genes that harbor such mutations, we selected four candidates carrying variants with a previously reported high probability of affecting protein function: *Smarcal1*, *Usp37*, Zinc finger protein 142 (*Zfp142*), and Serine/threonine-protein kinase 36 (*Stk36*) (Figure 4C).[31] We generated 3D protein structure models of these candidates to visualize the precise location of potentially high-impact gene variants (Figure 4D). Most allele variations could be found within flexible protein regions, while the USP37 allele variant (C244S) was located within a helical structure, which might be compromised in the B6 variant (Figure 4E). The localization of the identified allele variants in flexible and helical domains suggests that the binding affinity with interaction partners might be affected.

Interestingly, two candidates could affect PGB density through both changes in gene expression levels as well as through changes in protein function: the annealing helicase *Smarcal1* and the deubiquitinase *Usp37*.

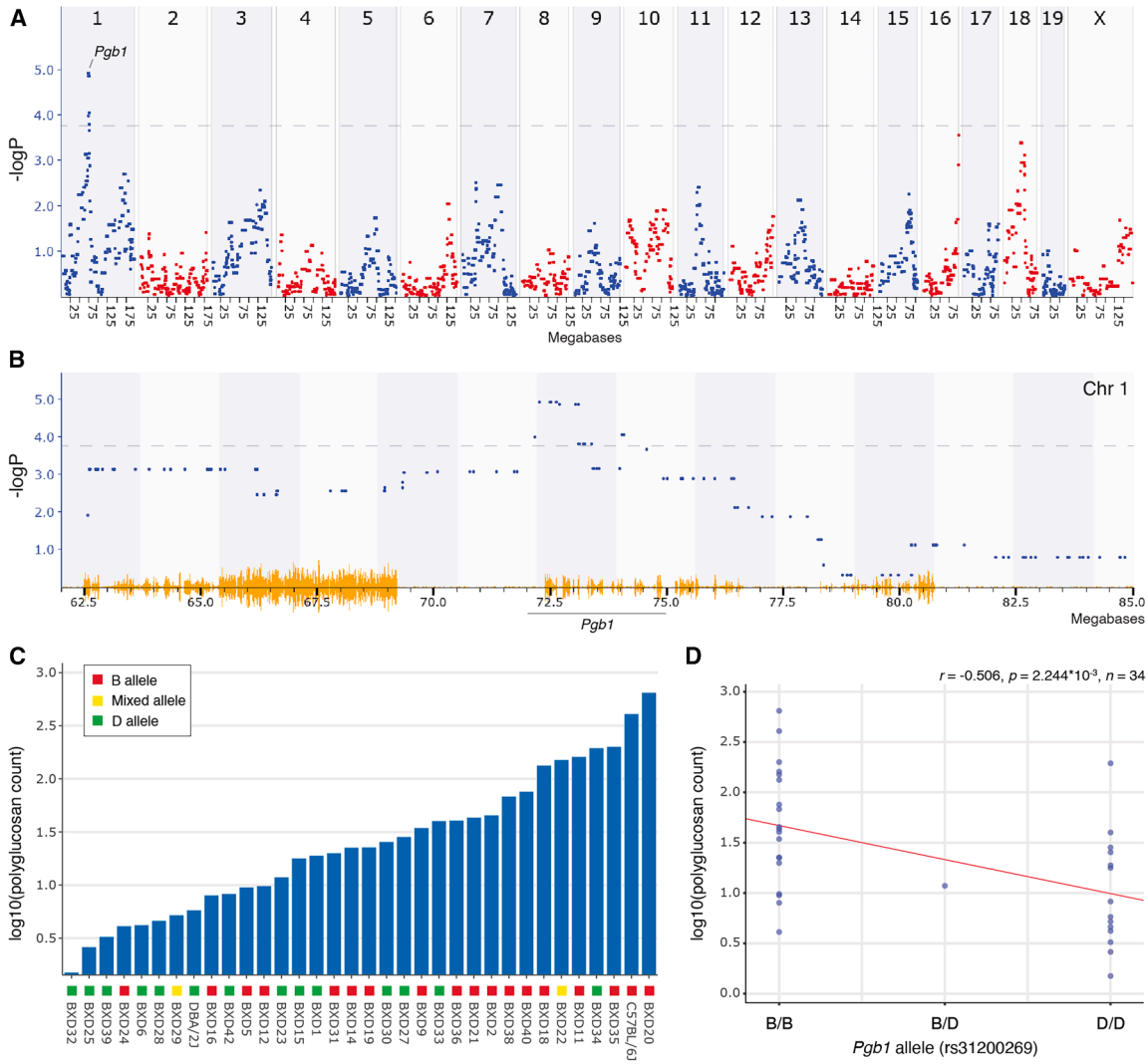

Figure 3. QTL mapping of PGB burden reveals a causal variation on chr 1

(A) Manhattan plot indicating the correlation significance between PGB densities (GeneNetwork trait: BXD_10686) and linkage blocks across the genome.

(B) Target region on chr 1, including the peak region of interest between 72 and 75 megabase (Mb). The yellow color indicates allele variations between BXD strains annotated at GeneNetwork.org. (A and B) The gray dotted line indicates genome-wide significance at −log *p* of 3.832.

(C) Log10 transformed average of PGBs per hippocampus of 32 BXD strains, as well as the parental strains C57BL/6J and DBA/2J. Mixed allele (yellow) indicates strains that contain both alleles in a homozygous manner (BB as well as DD) within the *Pgb1* locus (72–75 Mb). See also Figure S2.

(D) Pearson correlation between the *Pgb1* allele (using SNP marker rs31200269) and PGB burden. The heterozygous strain (B/D) is BXD23.

regulate *Smarcal1* (*n* = 198) and *Usp37* (*n* = 292) using the GeneHancer database.[34] We then cross-referenced these with 16 astrocyte-specific transcription factors identified by Yao et al. (module 43).[32] Interestingly, *Smarcal1* was predicted to be regulated by the astrocyte-specific transcription factor ETS variant transcription factor 4 (ETV4), while *Usp37* was predicted to be regulated by both ETV4 and SRY-box transcription factor 13 (SOX13). Fisher's exact test was used to assess the likelihood of finding such an overlap between the compared astrocyte-specific and *Smarcal1* or *Usp37* regulating gene lists by chance, which was negligible ($p < 4.44e{-}04$ and $p < 2.01e{-}07$, respectively). As ETV4 could regulate both *Smarcal1* and *Usp37*, we investigated the expression of *Etv4* in an independent single-cell RNA-sequencing dataset and confirmed that *Etv4* is specifically expressed in astrocytes (Figure S5A).[33] Furthermore, we found that *Etv4* shows a particularly high expression in aged (18-month-old) astrocytes when compared with their young (2-month-old) counterparts (Figure S5B). These findings suggest that astrocyte-specific transcription factors, particularly ETV4, may mediate the cell-type-specific and age-affected regulation of genes at the *Pgb1* locus.

Single-nucleus ATAC-sequencing reveals astrocyte-specific chromatin accessibility at the *Pgb1* locus

To further investigate whether chromatin regulation underlies the cell-type-specific expression of *Pgb1* locus genes, we analyzed chromatin accessibility using a single nucleus assay for transposase-accessible chromatin sequencing (snATACseq) dataset from mouse hippocampus at 3, 10, and 18 months of age.[35]

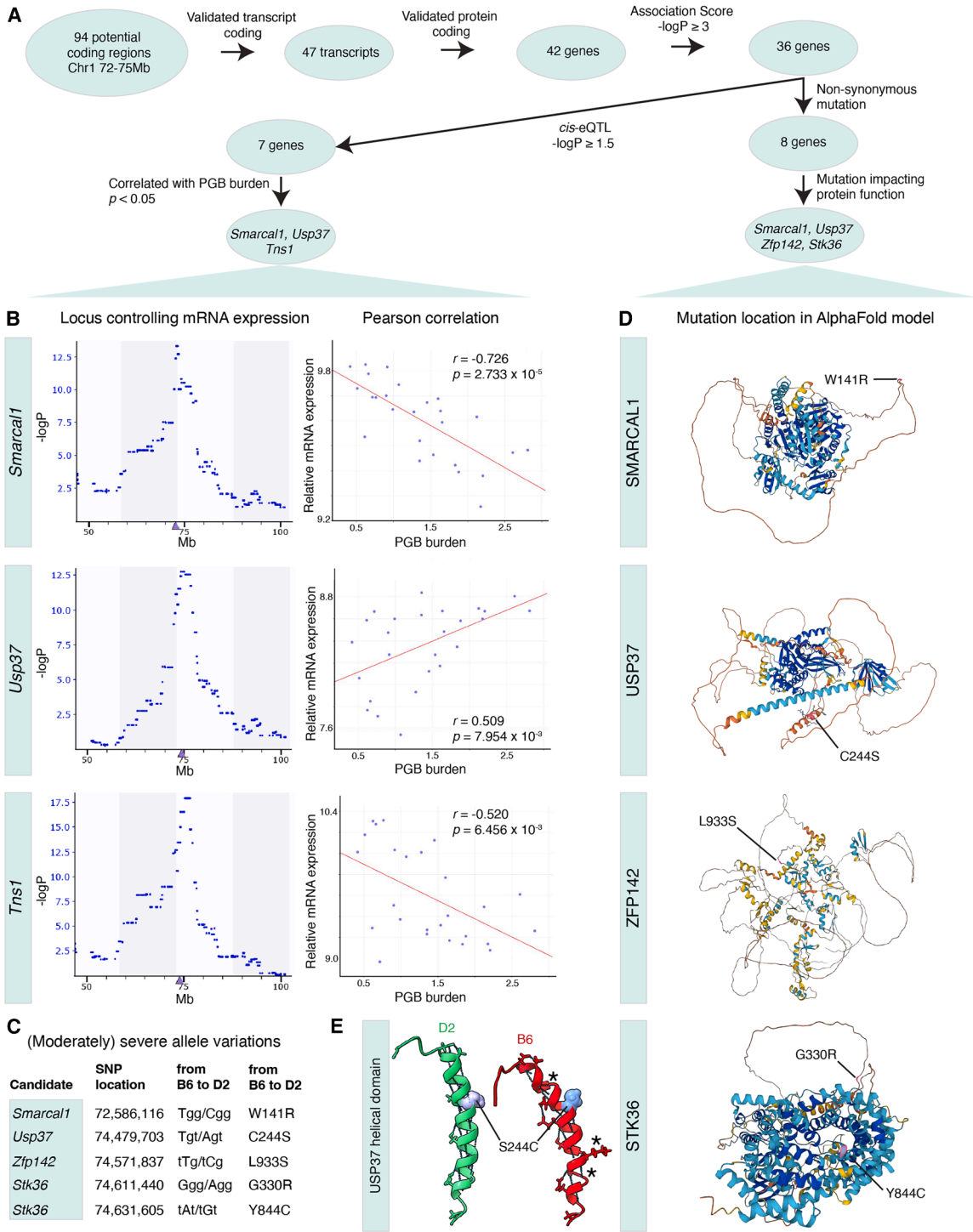

Figure 4. Selection of *Pgb1* candidate genes highlights potential impact of *Smarcal1*, *Usp37*, *Tns1*, *Zfp142*, and *Stk36* on PGB burden

(A) Workflow of candidate selection, which was performed employing data provided in Table S2.

(B) *Cis*-eQTL peak location (left) and correlation of candidate gene mRNA expression with PGB burden (right), which is defined as the log10-transformed average of PGBs per hippocampus. Pearson correlations were calculated from the mean values of 26 strains.

(C) List of (moderately) severe allele variations between the B and D alleles within candidate protein-coding genes (data extracted from Wang et al.[31]).

(D) AlphaFold protein structure prediction models of the candidate genes, produced using the Ensembl browser and genome assembly GRCm39. Indicated are the locations of the allele variations (pink) between the B6 and D2 strains listed in (C). Colors correspond to AlphaFold model confidence, ranging from very high (dark blue) and confident (cyan) to low (yellow) and very low (orange).

(E) Helical conformation in USP37, including the C244S allele variant, which impacts the helical integrity at locations indicated by the asterisks. Blue dashed lines indicate hydrogen bonds.

Table 1. *Trans*-acting regulatory effects of *Pgb1* on mRNA expression in the hippocampus

Gene	Location (Mb)	Functional association[a]	−log *p*	B/D[b]	r[c]	Effect size	Record ID
Hp1bp3	chr 4: 138.241495	heterochromatin organization	6.31	D	0.20	0.094	10340721
Ext2	chr 2: 93.695631	glycosyltransferase active at the Golgi/ER	4.19	B	0.08	0.072	10485225
Tspan3	chr 9: 56.131723	membrane complex stability	3.39	B	0.39	−0.039	10593842
Cd81	chr 7: 143.052795	membrane structure and regulation	3.32	B	0.10	0.056	10559261
Pacsin2	chr 15: 83.375607	intracellular vesicular transport	3.29	D	0.26	0.050	10430997
Eid2	chr 7: 28.267881	negative transcriptional regulator	3.19	D	0.29	−0.030	10551483
Fosb	chr 7: 19.302696	transcription factor complex	3.16	D	0.42	0.080	10560481
Mtap2	chr 1: 66.175329	microtubule cytoskeleton organization	2.68	B	0.28	0.032	10347036
Htr5a	chr 5: 27.841947	serotonin receptor	2.55	D	0.53	0.048	10520355

[a]Functional information derived from UniProt and Gene Ontology (UniProt Consortium, 2023; Aleksander et al.[37]).
[b]Allele that increases expression.
[c]Pearson correlation between PGB burden and mRNA expression.

Across the *Pgb1* locus, we observed an age-dependent decline in chromatin accessibility in neuronal cell types. By contrast, chromatin at this locus remained accessible in astrocytes at 10 and 18 months (Figure S6). Notably, the promoters of both *Smarcal1* and *Usp37* remained accessible in astrocytes across all time points (Figure S7).

Together, these results indicate that age- and astrocyte-specific chromatin accessibility might contribute toward a potential astrocyte-specific regulatory effect of the *Pgb1* locus.

Pgb1 locus genes are upregulated in APDAs

Given that not all hippocampal astrocytes express *Smarcal1* and *Usp37* equally (Figure S3), we considered whether expression of these genes might be enriched in a subset of astrocytes—specifically, the APDAs described by Lee et al., in which PGBs arise (Figure 1).[15] To test this, we examined whether *Pgb1* locus genes are differentially expressed in APDAs compared with other astrocyte subtypes or states (Figure S8). Based on the differential expression analysis performed by Lee et al. 10 out of the 42 genes located at the *Pgb1* locus—including *Smarcal1* and *Usp37*—were significantly upregulated in APDAs, while only one gene (*Fosb*) was found to be significantly downregulated.[15] Interestingly, the transcription factor *Etv4* (Figure S5) was also significantly upregulated in APDAs, which might underlie the increased expression of *Smarcal1* and *Usp37*.

In summary, our findings indicate that the *Pgb1* locus exhibits cell-type-specific accessibility and activity, particularly in APDAs, supporting the hypothesis that the *Pgb1* locus modulates PGB accumulation in a cell-autonomous manner.

Phenome-wide association identifies *Pgb1* as a *trans*-regulator of *Hp1bp3* mRNA expression and PYGB protein abundance

To evaluate whether the *Pgb1* locus has any *trans*-acting regulatory effects on the expression levels of mRNAs or proteins from genes located in different regions of the genome, we performed a phenome-wide association study (PheWAS). SNP rs31200269 was used as a surrogate marker for the *Pgb1* locus since this SNP marker has the highest association with PGB density. SNP rs31200269 is located on chr 1 at 72.626982 Mb (GRCm38 mm10 assembly) in intron 14 of *Smarcal1*.

We applied a PheWAS test with the aged hippocampal exon array data generated for 67 BXD strains and 234 mice, which matched the age at which PGB burden was measured (mean age of 18 months). The strongest *trans*-acting regulatory effect of *Pgb1* was found with the expression of the terminal exon of heterochromatin protein 1 binding protein 3 (*Hp1bp3*) (probe set 10340721) (Table 1). *Hp1bp3* is located on chr 4 and is a modulator of cognitive function and conditioned fear memory (CFM) in older BXD mice.[36] *Hp1bp3* expression in the aged hippocampus mapped to the *Pgb1* locus with a −log *p* of 6.3, showing higher expression in the *D* allele compared with the *B* allele (Figures S9A–S9C). PGB burden and *Hp1bp3* expression showed a negatively covarying trend ($r = -0.34$, $p = 0.088$, Pearson correlation) when correlating the data encompassing 26 BXD strains for which both mRNA and PGB cluster counts were available (Figure S9D). Expression of *Hp1bp3* increased as a function of age in a way consistent with linkage to PGB burden (Figure S9E; $r = 0.29$, $p < 1 \times 10^{-5}$).[10]

To detect whether *Pgb1* influences PGB burden through changes at the protein level, we utilized an available BXD liver proteome dataset.[38] In total, 51 proteins were identified to be regulated by the *Pgb1* locus, including several metabolism-associated proteins, including GALT, CKMT1, SLC27A5, GPD1, LDHD, PYGB, NDUFS1, and MRPL39 (Table S4). *Pgb1* regulation of target proteins might be tissue specific. Therefore, we generated a hippocampal proteome dataset using 205 BXD females (6–24 months of age; sample details in Williams et al.[38]) and performed a hippocampus-specific proteome-wide PheWAS. We surveyed 17,799 proteins to identify those being *trans*-regulated by the *Pgb1* locus. A total of 23 proteins showed linkage scores at *Pgb1* with a $-\log p \geq 2$ (Tables 2 and S4). Interestingly, two metabolism-associated proteins identified in the liver PheWAS were also regulated by *Pgb1* in the hippocampus: NADH:ubiquinone oxidoreductase core subunit S1 (NDUFS1) and Glycogen Phosphorylase B (PYGB) (Tables 2 and S4). NDUFS1 is an NADH dehydrogenase and a member of mitochondrial complex I, which plays a major role in cellular ATP production. PYGB is an enzyme known to play a role in glycogen metabolism and could therefore be directly involved in glycogen regulation in hippocampal astrocytes.[41,42] Although the role of PYGB in glycogen regulation in the brain remains largely unstudied, potential associations could be found

Table 2. *Trans*-acting regulatory effects of *Pgb1* on protein expression in the hippocampus

Protein	Location (Mb)	Functional association[a]	−log *p*	B/D[b]	r value[c]	*p* value[c]
RHOB	chr 12: 8.497758	signaling GTPase	4.13	B	−0.29	8.42×10^{-5}
GDI2	chr 13: 3.537321	GDP dissociation inhibitor	3.59	D	0.55	4.23×10^{-4}
UBA1	chr X: 20.235452	ubiquitin conjugation	3.53	B	–0.31	7.35×10^{-6}
NPEPPS	chr 11: 97.066948	aminopeptidase	3.27	B	−0.30	6.74×10^{-4}
DDX5	chr 11: 106.641669	RNA helicase	3.16	B	−0.31	6.07×10^{-4}
UBE2D2B	chr 5: 107.830161	ubiquitin conjugation	3.11	B	−0.24	5.65×10^{-4}
PI4KA	chr 16: 17.280350	PI 4-kinase	3.08	B	−0.49	9.80×10^{-4}
NDUFS1	chr 1: 63.161045	NADH dehydrogenase	2.99	D	0.84	0.002
PYGB	chr 11: 97.066948	glycogen mobilizer	2.55	B	−0.72	0.004

[a]Functional information derived from UniProt and Gene Ontology (UniProt Consortium;[39] Aleksander et al.[36]; Yao et al.[40]).
[b]Allele that is associated with increased protein abundance.
[c]r and *p* values of the Pearson correlation between the Pgb1 SNP marker rs31200269 and relative protein abundance.

between PYGB and PGB-disease-associated factors NHLRC1 and GBE1, known proteins underlying Lafora disease and APBD, respectively. PYGB is ubiquitinated by NHLRC1 in lung tissue, inducing a nuclear-specific function of PYGB to degrade glycogen.[43] Furthermore, STRING database network analysis (v.12.0) suggests that PYGB could be an (indirect) interaction partner of GBE1, considering their shared function in glycogen metabolism, their co-expression in human microarray data available on GEO (correlation = 0.807), and their colocalization in protein complexes suggested by anti-coimmunoprecipitation assay analyses.[44] Taken together, we identified nine transcripts and 23 proteins *trans*-regulated in the hippocampus by the *Pgb1* locus, through which *Pgb1* could affect PGB burden.

PGB burden and age-related cognitive decline are uncorrelated

To assess the impact of PGB burden on cognition, phenome-wide associations between *Pgb1* and all of approximately 12,000 phenotypes available at GeneNetwork.org were investigated.[45,46] Notably, only two behavioral traits were linked to the *Pgb1* locus, including the level of activity in a Y-maze in 8-month-old females ($r = -0.78$, $n = 23$; GeneNetwork trait: BXD_20820).[47] This trait mapped to chr 1 with a −log *p* score of 4.8 at the *Pgb1* locus. Considering that the QTL peak association localized outside the *Pgb1* locus, the trait likely mapped due to a distal variant not associated with PGB burden directly. The *Pgb1* marker also covaried with cocaine-induced stereotypy (chewing, rearing; GeneNetwork trait: BXD_10315) in young adults ($-\log p = 4.2$, $r = 0.57$, $n = 23$), which is not directly linked with age-related cognition.[48] Hence, we did not detect convincing evidence of an effector role for *Pgb1* on cognitive performance using existing data.

Transcriptomics were used to find potential correlations between the *Pgb1* locus and genes known to be involved in cognition. Differential expression analysis between *Pgb1 DD* and *BB* genotypes in mice older than 600 days showed that after adjusting the *p* values for multiple testing, only 12 differentially expressed genes (DEGs) were identified from which seven are located within the *Pgb1* locus (*p* adj. < 0.05, Table S5). The small number of *trans*-regulated DEGs ($n = 5$) suggests that the downstream effects of the *Pgb1* locus on the aged hippocampal transcriptome are limited.

To exclude any effects that the *Pgb1* locus might have on the expression of genes associated with cognition, we selected 995 DEGs using unadjusted *p* values < 0.05, of which only 35 showed a (−)logFC over 0.2. Among these DEGs, genes within the *Pgb1* locus *Tns1*, *Smarcal1*, and RUN and FYVE domain-containing protein 4 (*Rufy4*) had the highest *p* values ($p < 2.96 \times 10^{-13}$, $p < 1.44 \times 10^{-12}$, and $p < 6.78 \times 10^{-12}$, respectively) (Figure 5A). Next, we tested the overlap between the DEGs (excluding *Pgb1 cis*-regulated genes) and two cognition-associated gene lists from the Gene Ontology and Mammalian Phenotype repositories (GO:0050890_cognition and MP:0014114_abnormal_cognition, respectively) (Figures 5B and 5C; Table S6). Notably, no significant overlap was found, which indicates that the *Pgb1* locus does not affect transcriptomic changes associated with cognition in mice over 600 days old.

To further investigate the potential correlation between PGB burden and age-related cognitive decline, we performed CFM and Y-maze tests on 14-month-old BXDs from 42 different strains, which were backcrossed with C57BL/6J. Both males and females were used, which did not display sex-specific behavioral performances (Figure S10). At 14 months of age, PGBs are present in the B6 hippocampus, and age-related behavioral alterations such as reduced CFM become apparent.[10,49–51] As the effect of the C57BL/6J genotype on PGBs requires two copies of the B6-allele, which was shown in a previously published B6×D2 intercross study, approximately 50% of our cohort will possess a high-risk (*BB*) genotype and 50% a low-risk (*BD*) genotype.[52]

No correlation was found between CFM (time spent frozen) and PGB burden in the subset of overlapping strains ($r = 0.0561$; $p = 0.855$; $n = 13$ strains, GeneNetwork trait: 5XF_10474; Figures 5D–5F). No significant correlation was found between *Pgb1* and CFM when considering all 142 animals across 36 strains ($r = -0.100$; $p = 0.563$; $n = 36$ strains), showing that animals with a *Pgb1 BB* allele, which are expected to carry more PGBs, do not underperform compared with mice with a *Pgb1 BD* allele (Figures 5G and S11). We investigated the short-term spatial memory performance by Y-maze testing, for which we assessed the number of correct alternations defined as the subsequent investigation of previously uninvestigated arms of the maze (Figure 5H). No significant correlation was found between the percentage of correct alternations and PGB

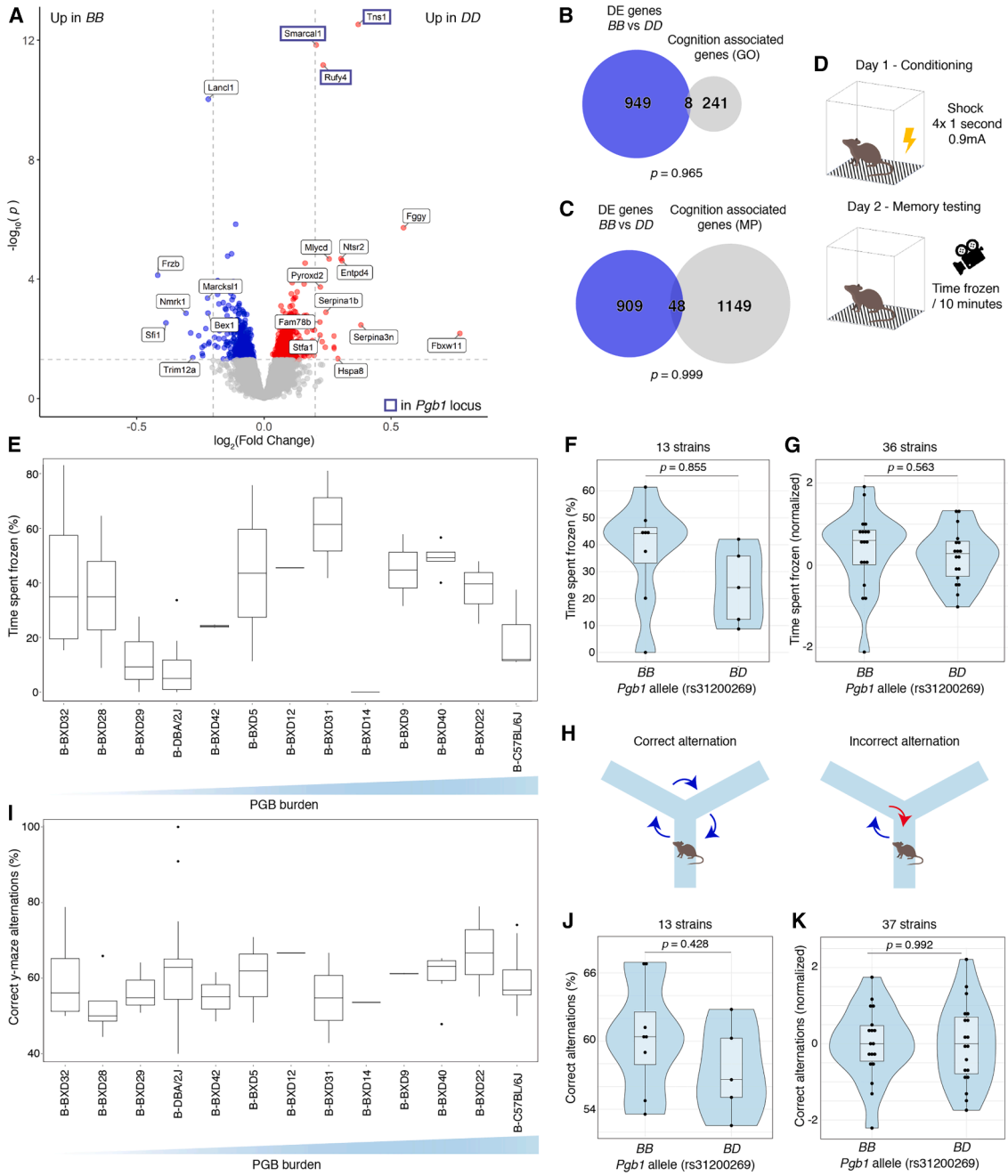

Figure 5. Cognitive capacity and PGB burden are uncorrelated in aged mice

(A) Volcano plot indicating DEGs between old mice (age > 600 days) with a BB or DD allele at the *Pgb1* locus, determined using the R package limma (eBayes function). Note that the three highest overexpressed genes in DD are localized within the *Pgb1* locus (highlighted by a dark blue box).

(B and C) DEGs (excluding genes located in the *Pgb1* locus) between old *BB* and *DD* carriers are not significantly enriched for genes known to be associated with cognitive performance. (B) GO:0050890_cognition and (C) MP:0014114_abnormal_cognition.

(D) Workflow of conditioned fear memory (CFM) test.

(E) Time spent frozen plotted for each strain, ordered from low to high PGB burden. All tested mice were 14 months of age and resulted from a backcross of homozygous BXD strains with the B parental strain.

(F) Time spent frozen (%) by *Pgb1* allele. Means per strain (n = 13) were used to account for variable numbers of mice used per strain. No significant correlation was found between the *Pgb1* allele and CFM score.

(G) Pearson correlation plotted showing normalized CFM score per allele at *Pgb1* (rs31200269). The data can be found under GeneNetwork.org trait: 5XF_10474. In total, 142 animals of 14 months of age were tested across 36 different strains.

(H) Workflow of Y-maze test.

(legend continued on next page)

burden (r = 0.241; p = 0.428; n = 13 strains; Figures 5I and 5J). Although the limited number of strains analyzed here (n = 13) provided sufficient power (0.7) to detect strong effect sizes (>0.8), it was insufficient to detect weaker effects. To address this, we expanded our analysis to assess the correlation between Y-maze performance and *Pgb1* allele inheritance in 164 animals spanning 37 strains. However, no significant correlation was observed between *Pgb1* and Y-maze performance (r = −0.002; p = 0.992; GeneNetwork trait: 5XF_10013; see Figures 5K and S12).

Collectively, the results of the phenome-wide association scans, the transcriptomic analysis, and the CFM and Y-maze behavioral tests did not provide any evidence suggesting a negative impact of PGBs on cognition.

DISCUSSION

In this study, we characterized the aged BXD mouse hippocampus in the context of PGB burden, using a plethora of complementary approaches, including histology, genomics, transcriptomics, proteomics, and behavioral testing. Our results identified the *Pgb1* locus that modulates PGB burden and have identified genes, mRNAs, and proteins implicated in the mechanism underlying PGB burden. In contrast to the detrimental role of PGBs in neurological diseases such as Lafora disease,[6,53–56] our results suggest that PGB accumulation in non-pathological contexts is more likely a neutral aspect of aging than a major cause of cognitive decline.

Quantification of PGB burden in the hippocampus of BXD mice revealed that PGB burden varies widely between strains, which is in accordance with previous studies that have shown that PGB abundance has a strong heritable component.[11] One of the major advantages of using the fully sequenced inbred BXD strains is the availability of cross-correlation between independently produced datasets.[57–60] Here, we leveraged pre-existing datasets and also generated new mRNA and protein expression data from the aged BXD hippocampus, which can be utilized by us and others to further investigate the genetics underlying hippocampal aging.

The transcriptomic dataset produced here was utilized to identify two protein-coding candidates likely to impact PGB burden, *Smarcal1* and *Usp37*. Both candidates harbor a non-synonymous mutation with the potential to impact protein function, and the mRNA expression levels of *Smarcal1* and *Usp37* significantly correlate with PGB burden. *Smarcal1* encodes an annealing helicase involved in repairing forked ends of DNA in response to DNA damage, and *Usp37* encodes a deubiquitinase with limited functional characterization, although interestingly, it may also be linked to the DNA damage response, a key hallmark of aging.[61–63] These candidate gene variants likely affect PGB burden through the *trans*-regulation of mRNAs or proteins prioritized here, including PYGB, which induces glycogen mobilization after ubiquitination by NHLRC1. Interestingly, mutations in NHLRC1 (also known as malin) can cause Lafora disease, a neurodegenerative disorder characterized by PGB accumulation.[5,42] Furthermore, STRING network analysis indicated a strong link, including experimentally determined physical interactions, between PYGB and GBE1, an important enzyme in glycogen synthesis and the underlying genetic cause of APBD.[2,3] The candidate genes, mRNAs, and proteins defined here are targets for follow-up studies aiming to identify the underlying mechanisms of PGB formation and degradation. For example, it seems plausible that NHLRC1, which ubiquitates PYGB to induce its catabolic activity, could be counteracted by deubiquitinase USP37, one of the major candidates located within the *Pgb1* locus.

Recent work has identified the age-related occurrence of APDAs in the hippocampus of C57BL/6 mice, which negatively affect synapse number and homeostasis of adjacent neurons.[15] Here, we show that PGBs arise in cells displaying APDA markers, SCRG1 and SQSTM1. The finding that PGBs arise in APDAs suggests that the accumulation of PGBs in astrocytes might be a downstream effect of compromised autophagy, a primary hallmark of aging.[23,64] While SCRG1/SQSTM1 antibody positivity defines APDAs, whether or not these antibodies bind their intended epitope in hippocampal astrocytes remains to be determined, as PGBs are known to induce antibody reactivity in an epitope-independent manner.[11,12,65]

Hippocampal astrocytes are known to participate actively during memory consolidation and the location-specific encoding of the reward system.[16–20] In addition, APDAs have been shown to reduce the number of synapses in adjacent neurons.[15] Therefore, we hypothesized that the occurrence of PGBs in hippocampal astrocytes might have negative consequences on brain health and cognition during non-pathological aging. Notably, we did not find any compelling evidence suggesting a negative impact of PGBs on cognition using phenome-wide association scans, transcriptomic analyses, and behavioral (CFM and Y-maze) cognition testing of aged BXDs. The lack of association between PGB burden and cognition may be analogous to increased non-pathological aggregation of protein observed during aging, largely due to a decline in proteostasis.[66] Emerging evidence suggests that insoluble protein aggregates, which are observed in aging as well as in many neurodegenerative disease states, are not particularly neurotoxic.[67,68] By contrast, small soluble misfolded oligomeric species are shown to contribute substantially to neurodegeneration.[69] Our results, which indicate that the effects of glycogen aggregation on age-related cognitive decline are limited, support the notion that aggregation is not always detrimental to cognition and health.

To accurately interpret our data, we need to consider compensation at both genetic and functional levels. Genetic compensation may have prevented us from identifying additional genes influencing PGB burden, as upregulation of redundant genes or pathways could mask their expression. In addition, while *Pgb1* inheritance and PGB burden showed little correlation with behavior, functional redundancy might obscure its effects on cognition. Indeed, mouse models of glycogen storage

(I) Correct Y-maze alternations plotted for each strain, ordered from low to high PGB burden. The same mice were used as described in (E).
(J) Correct Y-maze alternations by the *Pgb1* allele. Means per strain (n = 13) were used to account for variable numbers of mice used per strain.
(K) Pearson correlation plotted showing normalized correct Y-maze alternations per allele at Pgb1 (rs31200269). The data can be found under GeneNetwork.org trait: 5XF_10013. In total, 164 animals of 14 months of age were tested across 37 different strains.

diseases often exhibit compensatory metabolic adaptations that alleviate severe symptoms observed in humans.[70,71] For example, while mouse models of glycogen storage disease IX-Beta develop metabolic abnormalities, they do not display the severe neurological and cognitive impairments seen in humans.[72] These differences underscore the limitations of mouse models in accurately replicating human glycogen storage disease symptoms, particularly in neurological and cognitive domains, due to species-specific metabolic adaptations. Consequently, although we did not observe a relationship between *Pgb1*/PGB burden and cognition in aged mice, this finding may not directly translate to the human context.

In summary, this study integrates multimodal data derived from the BXD mouse family to deepen our understanding of the accumulation of PGBs in the aged hippocampus. PGBs were known to be detrimental to cognition in diseases such as APBD and Lafora disease, but whether this applied to age-related PGBs remained largely unknown. Here, we have identified a locus modulating age-related PGB burden and highlighted candidate genes, mRNAs, and proteins that are likely molecular components in the thus far elusive mechanism underlying age-related PGB accumulation. In addition, following extensive assessment of possible molecular and behavioral associations, we conclude that the physiological impact of PGB burden in these animals is likely unrelated to their cognitive performance.

RESOURCE AVAILABILITY

Lead contact

Further information and requests for resources and reagents should be directed to and will be fulfilled by the lead contact, Dennis E.M. de Bakker (dennisdebakker@hotmail.com).

Materials availability

This study did not generate new materials.

Data and code availability

- Data: the produced transcriptomic data have been deposited at https://www.ncbi.nlm.nih.gov/geo/query/acc.cgi?acc=GSE274733 (GSE274733) and are publicly available as of the date of publication. Accession numbers are listed in the key resources table. The produced proteomics data have been deposited at https://www.ebi.ac.uk/pride/ under Project Name: Systems Genetics of Normal Aging and Alzheimer's Disease and Project (PXD012044) and are publicly available as of the date of publication. Accession numbers are listed in the key resources table. The non-standardized data (e.g., PGB count data, Y-maze results, and CFM data) are available at GeneNetwork.org Exact locations are provided in Table S3. This paper analyzes existing, publicly available data. These accession numbers for the datasets are listed in the key resources table. All data reported in this paper will be shared by the lead contact upon request.
- Code: this paper does not report original code.
- Any additional information required to reanalyze the data reported in this paper is available from the lead contact upon request.

ACKNOWLEDGMENTS

We would like to thank the Summer School *Systems Genetics of Neural Ageing* for bringing us together and spurring our international collaboration. We would also like to acknowledge the funding for the Summer School 2022 from the e:Med Systems Medicine Program of the BMBF (Bundesministerium für Bildung und Forschung; German Ministry of Education and Research) to R.W.O. In addition, we would like to thank the FLI imaging core facility for their assistance. A.G.-P. is supported by Fundación Séneca, Región de Murcia, Spain (21259/FPI/19). D.E.M.d.B. is financed by a Rubicon scholarship (452021116) from the Dutch Research Council (NWO). This work was also supported by NIH NIA R01AG070913-01 (R.W.W.), R01AG075813-01 (D.G.A.), and R01AG075818 (C.K.). We acknowledge the help of Larry Mobraaten (Jackson Laboratory, Bar Harbor, MN) with the BXD strains and U. Obermüller for the help with the histology. For the purpose of open access, the authors have applied a CC BY public copyright license to all author-accepted manuscripts arising from this submission.

AUTHOR CONTRIBUTIONS

D.E.M.d.B., M.J., and R.W.W. conceptualized this study. A.G.-P., D.M.G., H.X.N., J.E.T., D.E.M.d.B., L.L., Y.X., D.G.A., C.K., G.K., J.K., O.O., R.A., and E.G.W. conducted formal analyses and designed visualizations. A.G.-P., D.M.G., H.X.N., J.E.T., D.E.M.d.B., and R.W.W. wrote the original draft, and all other authors reviewed and edited the manuscript. D.K.I., M.J., R.W.O., R.W.W., and D.E.M.d.B. provided supervision. M.J., R.W.O., and R.W.W. provided funding for this study.

DECLARATION OF INTERESTS

The authors declare no competing interests.

STAR★METHODS

Detailed methods are provided in the online version of this paper and include the following:

- KEY RESOURCES TABLE
- EXPERIMENTAL MODEL DETAILS
  - Mice models for PGB burden estimation
  - Mice models for transcriptomics data
- METHOD DETAILS
  - Tissue preparation for PGB assessment
  - Quantification of PGBs
  - Hippocampal transcriptome in older BXD animals
  - Hippocampal proteomics in older BXD animals
  - Quantitative trait mapping
  - Mapping mRNA expression
  - Identification of allele variations affecting protein function
  - Age associated gene expression changes
  - Assessing cell type specific expression
  - Contextual fear conditioning data collection
  - Y-maze data analysis
- QUANTIFICATION AND STATISTICAL ANALYSIS
  - Protein structure prediction
  - Differential expression analysis in older BXD animals
  - PGB burden impact on cognitive performance
  - Phenome-wide association analysis of the *Pgb1* locus

SUPPLEMENTAL INFORMATION

Supplemental information can be found online at https://doi.org/10.1016/j.cels.2025.101488.

Received: September 18, 2024
Revised: June 28, 2025
Accepted: December 5, 2025
Published: February 2, 2026

REFERENCES

1. Duran, J., Gruart, A., García-Rocha, M., Delgado-García, J.M., and Guinovart, J.J. (2014). Glycogen accumulation underlies neurodegeneration and autophagy impairment in Lafora disease. Hum. Mol. Genet. *23*, 3147–3156. https://doi.org/10.1093/hmg/ddu024.

2. Nitschke, S., Sullivan, M.A., Mitra, S., Marchioni, C.R., Lee, J.P.Y., Smith, B.H., Ahonen, S., Wu, J., Chown, E.E., Wang, P., et al. (2022). Glycogen synthase downregulation rescues the amylopectinosis of murine RBCK1 deficiency. Brain *145*, 2361–2377. https://doi.org/10.1093/brain/awac017.
3. Zebhauser, P.T., Cordts, I., Hengel, H., Haslinger, B., Lingor, P., Akman, H.O., Haack, T.B., and Deschauer, M. (2022). Characterization of cognitive impairment in adult polyglucosan body disease. J. Neurol. *269*, 2854–2861. https://doi.org/10.1007/s00415-022-10960-z.
4. Duran, J., and Guinovart, J.J. (2015). Brain glycogen in health and disease. Mol. Aspects Med. *46*, 70–77. https://doi.org/10.1016/j.mam.2015.08.007.
5. Gentry, M.S., Worby, C.A., and Dixon, J.E. (2005). Insights into Lafora disease: Malin is an E3 ubiquitin ligase that ubiquitinates and promotes the degradation of laforin. Proc. Natl. Acad. Sci. USA *102*, 8501–8506. https://doi.org/10.1073/pnas.0503285102.
6. Moreno-Estellés, M., Campos-Rodríguez, Á., Rubio-Villena, C., Kumarasinghe, L., Garcia-Gimeno, M.A., and Sanz, P. (2023). Deciphering the Polyglucosan Accumulation Present in Lafora Disease Using an Astrocytic Cellular Model. Int. J. Mol. Sci. *24*, 6020. https://doi.org/10.3390/ijms24076020.
7. Wang, W., Lohi, H., Skurat, A.V., DePaoli-Roach, A.A., Minassian, B.A., and Roach, P.J. (2007). Glycogen metabolism in tissues from a mouse model of Lafora disease. Arch. Biochem. Biophys. *457*, 264–269. https://doi.org/10.1016/j.abb.2006.10.017.
8. Rai, A., and Ganesh, S. (2019). Polyglucosan Bodies in Aged Brain and Neurodegeneration: Cause or Consequence? In Models, Molecules and Mechanisms in Biogerontology: Physiological Abnormalities, Diseases and Interventions, P.C. Rath, ed. (Springer), pp. 57–89. https://doi.org/10.1007/978-981-13-3585-3_4.
9. Riba, M., Augé, E., Campo-Sabariz, J., Moral-Anter, D., Molina-Porcel, L., Ximelis, T., Ferrer, R., Martín-Venegas, R., Pelegrí, C., and Vilaplana, J. (2019). Corpora amylacea act as containers that remove waste products from the brain. Proc. Natl. Acad. Sci. USA *116*, 26038–26048. https://doi.org/10.1073/pnas.1913741116.
10. Jucker, M., Walker, L.C., Schwarb, P., Hengemihle, J., Kuo, H., Snow, A.D., Bamert, F., and Ingram, D.K. (1994). Age-related deposition of glia-associated fibrillar material in brains of C57BL/6 mice. Neuroscience *60*, 875–889. https://doi.org/10.1016/0306-4522(94)90269-0.
11. Jucker, M., Walker, L.C., Kuo, H., Tian, M., and Ingram, D.K. (1994). Age-related fibrillar deposits in brains of C57BL/6 mice. A review of localization, staining characteristics, and strain specificity. Mol. Neurobiol. *9*, 125–133. https://doi.org/10.1007/BF02816112.
12. Jucker, M., Walker, L.C., Martin, L.J., Kitt, C.A., Kleinman, H.K., Ingram, D.K., and Price, D.L. (1992). Age-Associated Inclusions in Normal and Transgenic Mouse Brain. Science *255*, 1443–1445. https://doi.org/10.1126/science.1542796.
13. Palmer, A.L., and Ousman, S.S. (2018). Astrocytes and Aging. Front. Aging Neurosci. *10*, 337. https://doi.org/10.3389/fnagi.2018.00337.
14. Viana, J.F., Machado, J.L., Abreu, D.S., Veiga, A., Barsanti, S., Tavares, G., Martins, M., Sardinha, V.M., Guerra-Gomes, S., Domingos, C., et al. (2023). Astrocyte structural heterogeneity in the mouse hippocampus. Glia *71*, 1667–1682. https://doi.org/10.1002/glia.24362.
15. Lee, E., Jung, Y.-J., Park, Y.R., Lim, S., Choi, Y.-J., Lee, S.Y., Kim, C.H., Mun, J.Y., and Chung, W.-S. (2022). A distinct astrocyte subtype in the aging mouse brain characterized by impaired protein homeostasis. Nat Aging *2*, 726–741. https://doi.org/10.1038/s43587-022-00257-1.
16. Brazhe, A., Verisokin, A., Verveyko, D., and Postnov, D. (2023). Astrocytes: new evidence, new models, new roles. Biophys. Rev. *15*, 1303–1333. https://doi.org/10.1007/s12551-023-01145-7.
17. Curreli, S., Bonato, J., Romanzi, S., Panzeri, S., and Fellin, T. (2022). Complementary encoding of spatial information in hippocampal astrocytes. PLoS Biol. *20*, e3001530. https://doi.org/10.1371/journal.pbio.3001530.
18. Denizot, A., Arizono, M., Nägerl, U.V., Soula, H., and Berry, H. (2019). Simulation of calcium signaling in fine astrocytic processes: Effect of spatial properties on spontaneous activity. PLoS Comput. Biol. *15*, e1006795. https://doi.org/10.1371/journal.pcbi.1006795.
19. Doron, A., Rubin, A., Benmelech-Chovav, A., Benaim, N., Carmi, T., Refaeli, R., Novick, N., Kreisel, T., Ziv, Y., and Goshen, I. (2022). Hippocampal astrocytes encode reward location. Nature *609*, 772–778. https://doi.org/10.1038/s41586-022-05146-6.
20. Polykretis, I., and Michmizos, K.P. (2022). The role of astrocytes in place cell formation: A computational modeling study. J. Comput. Neurosci. *50*, 505–518. https://doi.org/10.1007/s10827-022-00828-6.
21. Peirce, J.L., Lu, L., Gu, J., Silver, L.M., and Williams, R.W. (2004). A new set of BXD recombinant inbred lines from advanced intercross populations in mice. BMC Genet. *5*, 7. https://doi.org/10.1186/1471-2156-5-7.
22. Taylor, B.A. (1978). Recombinant inbred strains: use in gene mapping. In Origins of Inbred Mice (Elsevier), pp. 423–438. https://doi.org/10.1016/B978-0-12-507850-4.50032-9.
23. Aman, Y., Schmauck-Medina, T., Hansen, M., Morimoto, R.I., Simon, A.K., Bjedov, I., Palikaras, K., Simonsen, A., Johansen, T., Tavernarakis, N., et al. (2021). Autophagy in healthy aging and disease. Nat Aging *1*, 634–650. https://doi.org/10.1038/s43587-021-00098-4.
24. Kakhlon, O., Vaknin, H., Mishra, K., D'Souza, J., Marisat, M., Sprecher, U., Wald-Altman, S., Dukhovny, A., Raviv, Y., Da'adoosh, B., et al. (2021). Alleviation of a polyglucosan storage disorder by enhancement of autophagic glycogen catabolism. EMBO Mol. Med. *13*, e14554. https://doi.org/10.15252/emmm.202114554.
25. Ashbrook, D.G., Arends, D., Prins, P., Mulligan, M.K., Roy, S., Williams, E.G., Lutz, C.M., Valenzuela, A., Bohl, C.J., Ingels, J.F., et al. (2021). A platform for experimental precision medicine: The extended BXD mouse family. Cell Syst. *12*, 235–247.e9. https://doi.org/10.1016/j.cels.2020.12.002.
26. Zhou, X., and Stephens, M. (2012). Genome-wide efficient mixed-model analysis for association studies. Nat. Genet. *44*, 821–824. https://doi.org/10.1038/ng.2310.
27. Villani, F., Sasani, T.A., Maksimov, M., Gunturkun, M.H., Ma, N., Ren, Y., Rothschild, D., Chen, H., Lu, L., Dumont, B.L., et al. (2022). Deep sequencing of a large family of isogenic mice enables complex variants discovery and accurate phenotype mapping. Preprint at bioRxiv. https://doi.org/10.1101/2022.04.21.489063.
28. Li, M., Su, S., Cai, W., Cao, J., Miao, X., Zang, W., Gao, S., Xu, Y., Yang, J., Tao, Y.-X., et al. (2020). Differentially Expressed Genes in the Brain of Aging Mice With Cognitive Alteration and Depression- and Anxiety-Like Behaviors. Front. Cell Dev. Biol. *8*, 814. https://doi.org/10.3389/fcell.2020.00814.
29. McLaren, W., Gil, L., Hunt, S.E., Riat, H.S., Ritchie, G.R.S., Thormann, A., Flicek, P., and Cunningham, F. (2016). The Ensembl Variant Effect Predictor. Genome Biol. *17*, 122. https://doi.org/10.1186/s13059-016-0974-4.
30. Cembrowski, M.S., Wang, L., Sugino, K., Shields, B.C., and Spruston, N. (2016). Hipposeq: a comprehensive RNA-seq database of gene expression in hippocampal principal neurons. eLife *5*, e14997. https://doi.org/10.7554/eLife.14997.
31. Wang, X., Pandey, A.K., Mulligan, M.K., Williams, E.G., Mozhui, K., Li, Z., Jovaisaite, V., Quarles, L.D., Xiao, Z., Huang, J., et al. (2016). Joint mouse–human phenome-wide association to test gene function and disease risk. Nat. Commun. *7*, 10464. https://doi.org/10.1038/ncomms10464.
32. Yao, Z., van Velthoven, C.T.J., Kunst, M., Zhang, M., McMillen, D., Lee, C., Jung, W., Goldy, J., Abdelhak, A., Aitken, M., et al. (2023). A high-resolution transcriptomic and spatial atlas of cell types in the whole mouse brain. Nature *624*, 317–332. https://doi.org/10.1038/s41586-023-06812-z.
33. Jin, K., Yao, Z., van Velthoven, C.T.J., Kaplan, E.S., Glattfelder, K., Barlow, S.T., Boyer, G., Carey, D., Casper, T., Chakka, A.B., et al. (2025). Brain-wide cell-type-specific transcriptomic signatures of healthy ageing in mice. Nature *638*, 182–196. https://doi.org/10.1038/s41586-024-08350-8.

34. Fishilevich, S., Nudel, R., Rappaport, N., Hadar, R., Plaschkes, I., Iny Stein, T., Rosen, N., Kohn, A., Twik, M., Safran, M., et al. (2017). GeneHancer: Genome-wide integration of enhancers and target genes in GeneCards. Database *2017*, bax028. https://doi.org/10.1093/database/bax028.

35. Zhang, Y., Amaral, M.L., Zhu, C., Grieco, S.F., Hou, X., Lin, L., Buchanan, J., Tong, L., Preissl, S., Xu, X., et al. (2022). Single-cell epigenome analysis reveals age-associated decay of heterochromatin domains in excitatory neurons in the mouse brain. Cell Res. *32*, 1008–1021. https://doi.org/10.1038/s41422-022-00719-6.

36. Neuner, S.M., Garfinkel, B.P., Wilmott, L.A., Ignatowska-Jankowska, B.M., Citri, A., Orly, J., Lu, L., Overall, R.W., Mulligan, M.K., Kempermann, G., et al. (2016). Systems genetics identifies Hp1bp3 as a novel modulator of cognitive aging. Neurobiol. Aging *46*, 58–67. https://doi.org/10.1016/j.neurobiolaging.2016.06.008.

37. Gene Ontology Consortium, Aleksander, S.A., Balhoff, J., Carbon, S., Cherry, J.M., Drabkin, H.J., Ebert, D., Feuermann, M., Gaudet, P., Harris, N.L., et al. (2023). The Gene Ontology knowledgebase in 2023. Genetics *224*, iyad031. https://doi.org/10.1093/genetics/iyad031.

38. Williams, E.G., Pfister, N., Roy, S., Statzer, C., Haverty, J., Ingels, J., Bohl, C., Hasan, M., Čuklina, J., Bühlmann, P., et al. (2022). Multiomic profiling of the liver across diets and age in a diverse mouse population. Cell Syst. *13*, 43–57.e6. https://doi.org/10.1016/j.cels.2021.09.005.

39. The UniProt Consortium (2023). UniProt: the Universal Protein Knowledgebase in 2023. Nucleic Acids Res. *51*, D523–D531. https://doi.org/10.1093/nar/gkac1052.

40. Yao, Z., Van Velthoven, Nguyen, T.N., Goldy, J., Sedeno-Cortes, A.E., Baftizadeh, F., Bertagnolli, D., Casper, T., Chiang, M., Crichton, K., et al. (2021). A taxonomy of transcriptomic cell types across the isocortex and hippocampal formation. Cell *184*, 3222–3241. https://doi.org/10.1016/j.cell.2021.04.021.

41. Brown, A.M. (2004). Brain glycogen re-awakened. J. Neurochem. *89*, 537–552. https://doi.org/10.1111/j.1471-4159.2004.02421.x.

42. Mathieu, C., Li de la Sierra-Gallay, I.L., Duval, R., Xu, X., Cocaign, A., Léger, T., Woffendin, G., Camadro, J.-M., Etchebest, C., Haouz, A., et al. (2016). Insights into Brain Glycogen Metabolism: The STRUCTURE OF HUMAN BRAIN Glycogen Phosphorylase. J. Biol. Chem. *291*, 18072–18083. https://doi.org/10.1074/jbc.M116.738898.

43. Sun, R.C., Dukhande, V.V., Zhou, Z., Young, L.E.A., Emanuelle, S., Brainson, C.F., and Gentry, M.S. (2019). Nuclear Glycogenolysis Modulates Histone Acetylation in Human Non-Small Cell Lung Cancers. Cell Metab. *30*, 903–916.e7. https://doi.org/10.1016/j.cmet.2019.08.014.

44. Huttlin, E.L., Bruckner, R.J., Paulo, J.A., Cannon, J.R., Ting, L., Baltier, K., Colby, G., Gebreab, F., Gygi, M.P., Parzen, H., et al. (2017). Architecture of the human interactome defines protein communities and disease networks. Nature *545*, 505–509. https://doi.org/10.1038/nature22366.

45. Mulligan, M.K., Mozhui, K., Prins, P., and Williams, R.W. (2017). GeneNetwork: A Toolbox for Systems Genetics. Methods Mol. Biol. *1488*, 75–120. https://doi.org/10.1007/978-1-4939-6427-7_4.

46. Sloan, Z., Arends, D., Broman, K.W., Centeno, A., Furlotte, N., Nijveen, H., Yan, L., Zhou, X., Williams, R.W., and Prins, P. (2016). GeneNetwork: framework for web-based genetics. J. Open Source Softw. *1*, 25. https://doi.org/10.21105/joss.00025.

47. Neuner, S.M., Heuer, S.E., Huentelman, M.J., O'Connell, K.M.S., and Kaczorowski, C.C. (2019). Harnessing Genetic Complexity to Enhance Translatability of Alzheimer's Disease Mouse Models: A Path toward Precision Medicine. Neuron *101*, 399–411.e5. https://doi.org/10.1016/j.neuron.2018.11.040.

48. Jones, B.C., Tarantino, L.M., Rodriguez, L.A., Reed, C.L., McClearn, G.E., Plomin, R., and Erwin, V.G. (1999). Quantitative-trait loci analysis of cocaine-related behaviours and neurochemistry. Pharmacogenetics *9*, 607–617. https://doi.org/10.1097/00008571-199910000-00007.

49. Amelchenko, E.M., Bezriadnov, D.V., Chekhov, O.A., Anokhin, K.V., Lazutkin, A.A., and Enikolopov, G. (2023). Age-related decline in cognitive flexibility is associated with the levels of hippocampal neurogenesis. Front. Neurosci. *17*, 1232670. https://doi.org/10.3389/fnins.2023.1232670.

50. Hamieh, A.M., Camperos, E., Hernier, A.M., and Castagné, V. (2021). C57BL/6 mice as a preclinical model to study age-related cognitive deficits: Executive functions impairment and inter-individual differences. Brain Res. *1751*, 147173. https://doi.org/10.1016/j.brainres.2020.147173.

51. Wu, M.V., Luna, V.M., and Hen, R. (2015). Running rescues a fear-based contextual discrimination deficit in aged mice. Front. Syst. Neurosci. *9*, 114. https://doi.org/10.3389/fnsys.2015.00114.

52. Krass, K.L., Colinayo, V., Ghazalpour, A., Vinters, H.V., Lusis, A.J., and Drake, T.A. (2003). Genetic loci contributing to age-related hippocampal lesions in mice. Neurobiol. Dis. *13*, 102–108. https://doi.org/10.1016/S0969-9961(03)00034-2.

53. Brewer, M.K., Putaux, J.-L., Rondon, A., Uittenbogaard, A., Sullivan, M.A., and Gentry, M.S. (2020). Polyglucosan body structure in Lafora disease. Carbohydr. Polym. *240*, 116260. https://doi.org/10.1016/j.carbpol.2020.116260.

54. Pederson, B.A., Turnbull, J., Epp, J.R., Weaver, S.A., Zhao, X., Pencea, N., Roach, P.J., Frankland, P.W., Ackerley, C.A., and Minassian, B.A. (2013). Inhibiting glycogen synthesis prevents Lafora disease in a mouse model. Ann. Neurol. *74*, 297–300. https://doi.org/10.1002/ana.23899.

55. Turnbull, J., Epp, J.R., Goldsmith, D., Zhao, X., Pencea, N., Wang, P., Frankland, P.W., Ackerley, C.A., and Minassian, B.A. (2014). PTG protein depletion rescues malin-deficient Lafora disease in mouse. Ann. Neurol. *75*, 442–446. https://doi.org/10.1002/ana.24104.

56. Turnbull, J., DePaoli-Roach, A.A., Zhao, X., Cortez, M.A., Pencea, N., Tiberia, E., Piliguian, M., Roach, P.J., Wang, P., Ackerley, C.A., et al. (2011). PTG depletion removes Lafora bodies and rescues the fatal epilepsy of Lafora disease. PLoS Genet. *7*, e1002037. https://doi.org/10.1371/journal.pgen.1002037.

57. Ashbrook, D.G., Williams, R.W., Lu, L., Stein, J.L., Hibar, D.P., Nichols, T.E., Medland, S.E., Thompson, P.M., and Hager, R. (2014). Joint genetic analysis of hippocampal size in mouse and human identifies a novel gene linked to neurodegenerative disease. BMC Genomics *15*, 850. https://doi.org/10.1186/1471-2164-15-850.

58. Chesler, E.J., Lu, L., Wang, J., Williams, R.W., and Manly, K.F. (2004). WebQTL: rapid exploratory analysis of gene expression and genetic networks for brain and behavior. Nat. Neurosci. *7*, 485–486. https://doi.org/10.1038/nn0504-485.

59. Kempermann, G., Chesler, E.J., Lu, L., Williams, R.W., and Gage, F.H. (2006). Natural variation and genetic covariance in adult hippocampal neurogenesis. Proc. Natl. Acad. Sci. USA *103*, 780–785. https://doi.org/10.1073/pnas.0510291103.

60. Lu, L., Airey, D.C., and Williams, R.W. (2001). Complex Trait Analysis of the Hippocampus: Mapping and Biometric Analysis of Two Novel Gene Loci with Specific Effects on Hippocampal Structure in Mice. J. Neurosci. *21*, 3503–3514. https://doi.org/10.1523/JNEUROSCI.21-10-03503.2001.

61. Bansal, R., Hussain, S., Chanana, U.B., Bisht, D., Goel, I., and Muthuswami, R. (2020). SMARCAL1, the annealing helicase and the transcriptional co-regulator. IUBMB Life *72*, 2080–2096. https://doi.org/10.1002/iub.2354.

62. Wu, C., Chang, Y., Chen, J., Su, Y., Li, L., Chen, Y., Li, Y., Wu, J., Huang, J., Zhao, F., et al. (2021). USP37 regulates DNA damage response through stabilizing and deubiquitinating BLM. Nucleic Acids Res. *49*, 11224–11240. https://doi.org/10.1093/nar/gkab842.

63. Schumacher, B., Pothof, J., Vijg, J., and Hoeijmakers, J.H.J. (2021). The central role of DNA damage in the ageing process. Nature *592*, 695–703. https://doi.org/10.1038/s41586-021-03307-7.

64. López-Otín, C., Blasco, M.A., Partridge, L., Serrano, M., and Kroemer, G. (2023). Hallmarks of aging: An expanding universe. Cell *186*, 243–278. https://doi.org/10.1016/j.cell.2022.11.001.

65. Baglietto-Vargas, D., Forner, S., Cai, L., Martini, A.C., Trujillo-Estrada, L., Swarup, V., Nguyen, M.M.T., Do Huynh, K., Javonillo, D.I., Tran, K.M., et al. (2021). Generation of a humanized Aβ expressing mouse demonstrating aspects of Alzheimer's disease-like pathology. Nat. Commun. *12*, 2421. https://doi.org/10.1038/s41467-021-22624-z.

66. David, D.C. (2012). Aging and the aggregating proteome. Front. Genet. *3*, 247. https://doi.org/10.3389/fgene.2012.00247.

67. Cuanalo-Contreras, K., Schulz, J., Mukherjee, A., Park, K.-W., Armijo, E., and Soto, C. (2023). Extensive accumulation of misfolded protein aggregates during natural aging and senescence. Front. Aging Neurosci. *14*, 1090109. https://doi.org/10.3389/fnagi.2022.1090109.

68. Wilson, D.M., Cookson, M.R., Van Den Bosch, L.V.D., Zetterberg, H., Holtzman, D.M., and Dewachter, I. (2023). Hallmarks of neurodegenerative diseases. Cell *186*, 693–714. https://doi.org/10.1016/j.cell.2022.12.032.

69. Rinauro, D.J., Chiti, F., Vendruscolo, M., and Limbocker, R. (2024). Misfolded protein oligomers: mechanisms of formation, cytotoxic effects, and pharmacological approaches against protein misfolding diseases. Mol. Neurodegener. *19*, 20. https://doi.org/10.1186/s13024-023-00651-2.

70. Gardin, A., Rouillon, J., Montalvo-Romeral, V., Rossiaud, L., Vidal, P., Launay, R., Vie, M., Krimi Benchekroun, Y.K., Cosette, J., Bertin, B., et al. (2024). A functional mini-GDE transgene corrects impairment in models of glycogen storage disease type III. J. Clin. Investig. *134*, e172018. https://doi.org/10.1172/JCI172018.

71. Sidman, R.L., Taksir, T., Fidler, J., Zhao, M., Dodge, J.C., Passini, M.A., Raben, N., Thurberg, B.L., Cheng, S.H., and Shihabuddin, L.S. (2008). Temporal Neuropathologic and Behavioral Phenotype of 6Neo/6Neo Pompe Disease Mice. J. Neuropathol. Exp. Neurol. *67*, 803–818. https://doi.org/10.1097/NEN.0b013e3181815994.

72. Arends, C.J., Wilson, L.H., Estrella, A., Kwon, O.S., Weinstein, D.A., and Lee, Y.M. (2022). A Mouse Model of Glycogen Storage Disease Type IX-Beta: A Role for Phkb in Glycogenolysis. Int. J. Mol. Sci. *23*, 9944. https://doi.org/10.3390/ijms23179944.

73. Gautier, L., Cope, L., Bolstad, B.M., and Irizarry, R.A. (2004). affy—analysis of Affymetrix GeneChip data at the probe level. Bioinformatics *20*, 307–315. https://doi.org/10.1093/bioinformatics/btg405.

74. Botía, J.A., Vandrovcova, J., Forabosco, P., Guelfi, S., D'Sa, K., United Kingdom; Brain; Expression Consortium, Hardy, J., Lewis, C.M., Ryten, M., and Weale, M.E. (2017). An additional k-means clustering step improves the biological features of WGCNA gene co-expression networks. BMC Syst. Biol. *11*, 47. https://doi.org/10.1186/s12918-017-0420-6.

75. Sturman, O., von Ziegler, L., Schläppi, C., Akyol, F., Privitera, M., Slominski, D., Grimm, C., Thieren, L., Zerbi, V., Grewe, B., et al. (2020). Deep learning-based behavioral analysis reaches human accuracy and is capable of outperforming commercial solutions. Neuropsychopharmacology *45*, 1942–1952. https://doi.org/10.1038/s41386-020-0776-y.

76. Love, M.I., Huber, W., and Anders, S. (2014). Moderated estimation of fold change and dispersion for RNA-seq data with DESeq2. Genome Biol. *15*, 550. https://doi.org/10.1186/s13059-014-0550-8.

77. Harrison, P.W., Amode, M.R., Austine-Orimoloye, O., Azov, A.G., Barba, M., Barnes, I., Becker, A., Bennett, R., Berry, A., Bhai, J., et al. (2024). Ensembl 2024. Nucleic Acids Res. *52*, D891–D899. https://doi.org/10.1093/nar/gkad1049.

78. Chen, S., Zhou, Y., Chen, Y., and Gu, J. (2018). fastp: an ultra-fast all-in-one FASTQ preprocessor. Bioinformatics *34*, i884–i890. https://doi.org/10.1093/bioinformatics/bty560.

79. Ritchie, M.E., Phipson, B., Wu, D., Hu, Y., Law, C.W., Shi, W., and Smyth, G.K. (2015). limma powers differential expression analyses for RNA-sequencing and microarray studies. Nucleic Acids Res. *43*, e47. https://doi.org/10.1093/nar/gkv007.

80. Jumper, J., Evans, R., Pritzel, A., Green, T., Figurnov, M., Ronneberger, O., Tunyasuvunakool, K., Bates, R., Žídek, A., Potapenko, A., et al. (2021). Highly accurate protein structure prediction with AlphaFold. Nature *596*, 583–589. https://doi.org/10.1038/s41586-021-03819-2.

81. Patro, R., Duggal, G., Love, M.I., Irizarry, R.A., and Kingsford, C. (2017). Salmon provides fast and bias-aware quantification of transcript expression. Nat. Methods *14*, 417–419. https://doi.org/10.1038/nmeth.4197.

82. Wolf, F.A., Angerer, P., and Theis, F.J. (2018). SCANPY: large-scale single-cell gene expression data analysis. Genome Biol. *19*, 15. https://doi.org/10.1186/s13059-017-1382-0.

83. Soneson, C., Love, M.I., and Robinson, M.D. (2015). Differential analyses for RNA-seq: transcript-level estimates improve gene-level inferences. F1000Res *4*, 1521. https://doi.org/10.12688/f1000research.7563.2.

84. Kent, W.J., Sugnet, C.W., Furey, T.S., Roskin, K.M., Pringle, T.H., Zahler, A.M., and Haussler, D. (2002). The human genome browser at UCSC. Genome Res. *12*, 996–1006. https://doi.org/10.1101/gr.229102.

85. Smith, C.L., and Eppig, J.T. (2009). The mammalian phenotype ontology: enabling robust annotation and comparative analysis. Wiley Interdiscip. Rev., Syst. Biol. Med. *1*, 390–399. https://doi.org/10.1002/wsbm.44.

86. Manich, G., Cabezón, I., Augé, E., Pelegrí, C., and Vilaplana, J. (2016). Periodic acid-Schiff granules in the brain of aged mice: From amyloid aggregates to degenerative structures containing neo-epitopes. Ageing Res. Rev. *27*, 42–55. https://doi.org/10.1016/j.arr.2016.03.001.

87. Kuo, H., Ingram, D.K., Walker, L.C., Tian, M., Hengemihle, J.M., and Jucker, M. (1996). Similarities in the age-related hippocampal deposition of periodic acid-schiff-positive granules in the senescence-accelerated mouse P8 and C57BL/6 mouse strains. Neuroscience *74*, 733–740. https://doi.org/10.1016/0306-4522(96)00169-8.

88. Geisert, E.E., Lu, L., Freeman-Anderson, N.E., Templeton, J.P., Nassr, M., Wang, X., Gu, W., Jiao, Y., and Williams, R.W. (2009). Gene Expression in the Mouse Eye: an Online Resource for Genetics Using 103 Strains of Mice. Mol Vis *15*, 1730–1763. https://pubmed.ncbi.nlm.nih.gov/19727342/.

89. Wu, Y., Williams, E.G., and Aebersold, R. (2017). Application of SWATH Proteomics to Mouse Biology. Current Protocols in Mouse Biology *7*, 130–143. https://doi.org/10.1002/cpmo.28.

90. Sasani, T.A., Ashbrook, D.G., Beichman, A.C., Lu, L., Palmer, A.A., Williams, R.W., Pritchard, J.K., and Harris, K. (2022). A natural mutator allele shapes mutation spectrum variation in mice. Nature *605*, 497–502. https://doi.org/10.1038/s41586-022-04701-5.

91. Yang, J., Zaitlen, N.A., Goddard, M.E., Visscher, P.M., and Price, A.L. (2014). Advantages and pitfalls in the application of mixed-model association methods. Nat. Genet. *46*, 100–106. https://doi.org/10.1038/ng.2876.

92. Beavis, W.D. (1994). The power and deceit of QTL experiments: lessons from comparative QTL studies. In Proceedings of the Forty-Ninth Annual Corn and Sorghum Industry Research Conference, pp. 252–268.

93. Beavis, W.D., Grant, D., Albertsen, M., and Fincher, R. (1991). Quantitative trait loci for plant height in four maize populations and their associations with qualitative genetic loci. Theor. Appl. Genet. *83*, 141–145. https://doi.org/10.1007/BF00226242.

94. Xu, S. (2003). Theoretical basis of the Beavis effect. Genetics *165*, 2259–2268. https://doi.org/10.1093/genetics/165.4.2259.

95. Westra, H.-J., and Franke, L. (2014). From genome to function by studying eQTLs. Biochim. Biophys. Acta *1842*, 1896–1902. https://doi.org/10.1016/j.bbadis.2014.04.024.

96. Kent, W.J. (2002). BLAT—The BLAST-Like Alignment Tool. Genome Res. *12*, 656–664. https://doi.org/10.1101/gr.229202.

97. Hernández-Mercado, K., and Zepeda, A. (2022). Morris Water Maze and Contextual Fear Conditioning Tasks to Evaluate Cognitive Functions Associated With Adult Hippocampal Neurogenesis. Front. Neurosci. *15*, 782947. https://doi.org/10.3389/fnins.2021.782947.

98. Verbitsky, M., Yonan, A.L., Malleret, G., Kandel, E.R., Gilliam, T.C., and Pavlidis, P. (2004). Altered Hippocampal Transcript Profile Accompanies an Age-Related Spatial Memory Deficit in Mice. Learn. Mem. *11*, 253–260. https://doi.org/10.1101/lm.68204.

99. Mathis, A., Mamidanna, P., Cury, K.M., Abe, T., Murthy, V.N., Mathis, M.W., and Bethge, M. (2018). DeepLabCut: markerless pose estimation of user-defined body parts with deep learning. Nat. Neurosci. *21*, 1281–1289. https://doi.org/10.1038/s41593-018-0209-y.

STAR★METHODS

KEY RESOURCES TABLE

REAGENT or RESOURCE	SOURCE	IDENTIFIER
Antibodies		
Antibody against laminin-binding protein 110 (LBP110)	Jucker et al.[10]	N/A
Goat anti-rabbit IgG	Jucker et al.[11]	*RRID:* AB_10122492
Biological samples		
Mice hippocampal tissue	This paper	BXD_10685
Mice whole cortex tissue	Yao et al., 2021	N/A
Mice hippocampal tissue	Cembrowski et al.[30]	N/A
Mice hippocampal tissue	Li et al.[28]	N/A
Mice liver tissue	Williams et al.[38]	GN888
Chemicals, peptides, and recombinant proteins		
diaminobenzidine		N/A
Critical commercial assays		
Vectastain Elite ABC Kit	Vector Laboratories	PK-6100
RNeasy mini kit	Qiagen	ID. 74104
Deposited data		
Raw PGB counts from the hippocampus	This paper	BXD_10685, see also Table S3
Log transformed PGB counts from the hippocampus	This paper	BXD_10686, see also Table S3
Hippocampal transcriptome (batch 1)	This paper	GN392
Hippocampal transcriptome (all batches)	This paper	GN712, GSE274733
Hippocampal bulk RNA-seq data	Li et al.[28]	SRP271007
Hippocampal proteome	This paper	GN873, PXD012044
Liver proteome	Williams et al.[38]	GN888
Whole cortex scRNA-seq data (10XGenomics)	Yao et al., 2021	RRID: SCR_002978
Whole cortex scRNA-seq data (Smart-Seq)	Yao et al., 2021	RRID: SCR_002978
Hippocampal scRNA-seq data	Cembrowski et al.[30]	GEO: GSE74985
Whole brain scRNA-seq data	Yao et al.[32]	SCR_015820
Whole brain scRNA-seq data	Jin et al.[33]	nemo:dat-61kfys3
Hippocampal scRNA-seq data	Lee at al.[15]	GEO: GSE183042
snATAC-seq from brain, heart, muscle, bone marrow	Zhang et al.[35]	GEO: GSE187332
Mutations segregating in the BXD family	Wang et al.[31]	Data S5; see also Table S3
Mutations segregating in the BXD family	Villani et al.[27]	Table S1; see also Table S3
Conditioned fear memory	This paper	5XF_10474, see also Table S3
Y-maze behavioral evaluation	This paper	5XF_10013, see also Table S3
Experimental models: Organisms/strains		
Mouse: BXD1/TyJ	The Jackson Laboratory	RRID: IMSR_JAX:000036
Mouse: BXD2/TyJ	The Jackson Laboratory	RRID: IMSR_JAX:000075
Mouse: BXD5/TyJ	The Jackson Laboratory	RRID: IMSR_JAX:000037
Mouse: BXD6/TyJ	The Jackson Laboratory	RRID: IMSR_JAX:000007
Mouse: BXD9/TyJ	The Jackson Laboratory	RRID: IMSR_JAX:000105
Mouse: BXD11/TyJ	The Jackson Laboratory	RRID: IMSR_JAX:000012
Mouse: BXD12/TyJ	The Jackson Laboratory	RRID: IMSR_JAX:000045
Mouse: BXD14/TyJ	The Jackson Laboratory	RRID: IMSR_JAX:000329

(*Continued on next page*)

Continued

REAGENT or RESOURCE	SOURCE	IDENTIFIER
Mouse: BXD15/TyJ	The Jackson Laboratory	RRID: IMSR_JAX:000095
Mouse: BXD16/TyJ	The Jackson Laboratory	RRID: IMSR_JAX:000013
Mouse: BXD18/TyJ	The Jackson Laboratory	RRID: IMSR_JAX:000015
Mouse: BXD19/TyJ	The Jackson Laboratory	RRID: IMSR_JAX:000010
Mouse: BXD20/TyJ	The Jackson Laboratory	RRID: IMSR_JAX:000330
Mouse: BXD21/TyJ	The Jackson Laboratory	RRID: IMSR_JAX:000077
Mouse: BXD22/TyJ	The Jackson Laboratory	RRID: IMSR_JAX:000043
Mouse: BXD23/TyJ	The Jackson Laboratory	RRID: IMSR_JAX:000098
Mouse: BXD24/TyJ	The Jackson Laboratory	RRID: IMSR_JAX:005243
Mouse: BXD25/TyJ	The Jackson Laboratory	RRID: IMSR_JAX:000081
Mouse: BXD27/TyJ	The Jackson Laboratory	RRID: IMSR_JAX:000041
Mouse: BXD28/TyJ	The Jackson Laboratory	RRID: IMSR_JAX:000047
Mouse: BXD29/Ty	The Jackson Laboratory	RRID: IMSR_JAX:010981
Mouse: BXD30	The Jackson Laboratory	N/A
Mouse: BXD31/TyJ	The Jackson Laboratory	RRID: IMSR_JAX:000083
Mouse: BXD32/TyJ	The Jackson Laboratory	RRID: IMSR_JAX:000078
Mouse: BXD34/TyJ	The Jackson Laboratory	RRID: IMSR_JAX:003223
Mouse: BXD38/TyJ	The Jackson Laboratory	RRID: IMSR_JAX:003227
Mouse: BXD39/TyJ	The Jackson Laboratory	RRID: IMSR_JAX:003228
Mouse: BXD40/TyJ	The Jackson Laboratory	RRID: IMSR_JAX:003229
Mouse: BXD42/TyJ	The Jackson Laboratory	RRID: IMSR_JAX:003230
Mouse: C57BL/6J	The Jackson Laboratory	RRID: IMSR_JAX:000664
Mouse: DBA/2J	The Jackson Laboratory	RRID: IMSR_JAX:000671
Mouse: B6-BXDF1s	The Jackson Laboratory	N/A
Software and algorithms		
affy R package	Gautier et al.[73]	https://bioconductor.org/packages/release/bioc/html/affy.html
Affymetrix GeneChip Operating Software	Affymetrix	RRID: SCR_003408
CoExpNets R package	Botía et al.[74]	https://github.com/juanbot/CoExpNets
DeeLabCut	Sturman et al.[75]	https://github.com/DeepLabCut/DeepLabCut
DESeq2	Love et al.[76]	https://bioconductor.org/packages/release/bioc/html/DESeq2.html
DLCAnalyzer	Sturman et al.[75]	https://github.com/ETHZ-INS/DLCAnalyzer
Ensembl Variant Effect Predictor	McLaren et al.[29]	Affymetrix GeneChip Operating Software
Ensembl web browser AlphaFold model	Harrison et al.[77]	https://alphafold.ebi.ac.uk/
fastp	Chen at al.[78]	https://github.com/OpenGene/fastp
GEMMA	Zhou and Stephens[26]	https://github.com/genetics-statistics/GEMMA
GeneNetwork	Mulligan al.[45]	https://genenetwork.org/
limma R package	Ritchie at al.[79]	https://bioconductor.org/packages/release/bioc/html/limma.html
local AlphaFold model	Jumper at al.[80]	https://github.com/deepmind/alphafold
Salmon	Patro et al.[81]	https://github.com/COMBINE-lab/salmon
scanpy	Wolf et al.[82]	https://scanpy.readthedocs.io/en/stable/
tximport	Soneson et al.[83]	https://bioconductor.org/packages/release/bioc/html/tximport.html
UCSC Genome Browser	Kent et al.[84]	https://genome.ucsc.edu/

(*Continued on next page*)

Continued

REAGENT or RESOURCE	SOURCE	IDENTIFIER
Other		
TCS SP8 X White Light Laser confocal microscope	Leica microsystems	https://www.leica-microsystems.com/products/confocal-microscopes/p/leica-tcs-sp8-x/
Bioanalyzer 2100	Agilent	https://www.agilent.com/en/product/automated-electrophoresis/bioanalyzer-systems/bioanalyzer-instrument/2100-bioanalyzer-instrument-228250
Affymetrix Mouse Gene 1.0 ST exon-style microarray	Affymetrix	901168
Gene Ontology	Gene Ontology Consortium[37]	https://geneontology.org/
Mammalian Phenotype	Smith and Eppig[85]	https://www.informatics.jax.org/vocab/mp_ontology

EXPERIMENTAL MODEL DETAILS

Mice models for PGB burden estimation

Mice used for the assessment of PGBs were obtained as retired breeders between 1997 and 1999 from The Jackson Laboratory (Bar Harbor) and further aged at the Gerontology Research Center, NIA, NIH. A total of 144 female mice (all 17-19 months of age) were used: 32 BXD strains (n=133; 2 to 10 mice/strain; mean 4.1/strain; RRID:MGI:2164899), C57BL/6J (n=4; RRID:IMSR_JAX:000664) and DBA/2J (n=5; RRID:IMSR_JAX:000671) (Table S3). BXDs are progeny of crosses of female C57BL/6J (B6 or B) and male DBA/2J (D2 or D) parents. Animals were euthanized by pentobarbital overdose and perfused transcardially with 0.1 M phosphate-buffered saline (PBS) at pH 7.4.

Mice models for transcriptomics data

234 individual mice (140 females and 94 males) from 71 BXD strains, parental C57BL/6J, DBA/2J and D2B6F1 hybrid, were used in producing the hippocampal transcriptome dataset (GN712) (Table S3). These mice were obtained from UTHSC, ORNL, Beth Israel Deaconess or directly from the Jackson Laboratory. The majority of mice were aged between 12 and 28 months (average of 18 months). The animals were euthanized under saturated isoflurane, and brains were removed and placed in RNAlater prior to dissection.

METHOD DETAILS

Tissue preparation for PGB assessment

Brains were removed and immersion fixed in 4% paraformaldehyde, followed by 30% sucrose, and freezing in isopentane at -20°C. Coronal sections throughout the hippocampus were cut on a freezing-sliding microtome at 25 μm. Visualization of PGBs was done as previously described.[10] In short, free-floating sections were rinsed with TBS (0.05 M Tris-buffer containing 1.5% NaCl, pH 7.4) and subsequently incubated in 0.3% Triton X-100 in TBS, followed by an incubation in 5% goat serum in TBS. Sections were reacted for two days at 4°C with an antibody against laminin-binding protein 110 (LBP110) in TBS containing 2% blocking serum and 0.3% Triton X-100, followed by secondary antibody labelling using goat anti-rabbit IgG. Antibodies were then detected by the ABC method with reagents from Vector Laboratories (Vectastain Elite ABC Kit, Vector Laboratories, Burlingame, CA, U.S.A.). The chromogen was diaminobenzidine, and the reaction product was intensified by adding NiCl. Fluorescent immunohistochemistry co-labeling LBP110 and p62/SQSTM1 was performed through an independent protocol (dx.doi.org/10.17504/protocols.io.kqdg32b47v25/v1) described in detail at protocols.io, and imaged using Leica's TCS SP8 X White Light Laser confocal microscope.

Quantification of PGBs

PGBs are typically detected with periodic acid-Schiff staining.[11,12,86] However, an antibody raised against the laminin-binding protein 110 (LBP110) was found to strongly bind PGB-lesions at light and ultrastructural levels and is largely used to identify PBGs in histological preparations.[11,12,87] The number of PGB clusters was assessed in a random systematic sampled set of every tenth section through the entire hippocampus. The total number of clusters of LBP110-positive PGBs per unilateral hippocampus was estimated by counting all PGB clusters in all sections and multiplying the number with the section sample fraction (10 for the present analysis). The PGB numbers among strains were strongly skewed (GeneNetwork trait ID: BXD_10685) and values were therefore $\log_{10}$ transformed prior to mapping (GeneNetwork trait ID: BXD_10686).

Hippocampal transcriptome in older BXD animals

Cerebella and olfactory bulbs from 234 individual mice (GN712) were removed; brains were hemisected, and both hippocampi were dissected whole in Dr. Lu's lab. Hippocampal samples were close to complete (see Lu et al., 2001), yet may include variable amounts of subiculum and fimbria.[60] All procedures were approved by the UTHSC Institutional Animal Care and Use Committee. RNA was extracted using the RNeasy mini kit (Qiagen, Valencia, CA, USA) according to the manufactures' instructions. RNA purity and concentration was assessed using 260/280 nm absorbance ratio, and RNA integrity was analyzed using the Agilent Bioanalyzer 2100 (Agilent Technologies). Samples with RNA Integrity Numbers (RIN values) > 7.5 were run on Affy MoGene1.0 ST at the UTHSC. This array contains 34,700 probe sets that target ~29,000 well-defined transcripts (RefSeq mRNA isoforms). A single probe is a collection of approximately 27 probes that target known exons within a single gene. The multiple probe design provides a more comprehensive coverage of transcripts from a single gene. Probe set level intensity values were extracted from CEL files using the Affymetrix GeneChip Operating Software (RRID:SCR_003408). Data normalization was performed as previously described, using the R package "affy" (RRID:SCR_012835).[73,88] The Robust Multichip Averaging protocol was used to process the expression values and the array data were then log transformed and rescaled using a z-scoring procedure to set the mean of each sample at eight expression units with a standard deviation (SD) of two units.

Hippocampal proteomics in older BXD animals

Hippocampal samples from 244 male and female mice from 40 BXD strains ranging in age from 2 to 37 months old were provided by CCK and LL. These samples were shipped from UTHSC to ETH Zurich for proteomic analysis (EGW, RA). Samples were processed according to the protocol online entitled "Application of SWATH Proteomics to Mouse Biology".[89] In brief, total proteome was first isolated using a RIPA-M buffer and then further lysed with a 8M urea buffer. After proteins were isolated, samples were trypsin digested overnight in the dark (approximately 22 hours @ 37 C in a mild shaker) in a 1.5M urea buffer followed by reduction by dithioethreitol and alkylation by iodoacetamide. Last, the peptides were passed through a C18 column and eluted in a 2% ACN solution with 0.1% FA. Samples were then loaded onto Evotips and separated with an Evosep liquid chromatographer coupled to a TripleTOF 5600 acquiring in SWATH mode on a one-hour gradient with 56 windows. The data is available in the PRIDE database under identifier PXD012044.

Quantitative trait mapping

Two datasets were generated. The original untransformed dataset for 32 members of the BXD family (GeneNetwork trait BXD_10685) had a range of values from almost free of any polyglucosan aggregates (1.5 PGBs per hippocampus on average in BXD32) to very high densities of PGBs (646 PGBs per hippocampus on average in BXD20). Due to the extreme skew (3.3) and kurtosis (12) the original data were not well suited for mapping (Figure S1). However, $\log_{10}$ transformed data (GeneNetwork trait BXD_10686) were suitable for mapping and have low skew (0.29) and kurtosis (–0.58) and mean and median are both approximately 1.4 (Figure 3C). We used existing whole-genome sequence (WGS) marker maps and the GRCm38 (mm10) mouse assembly.[25,90] These high density genetic maps were used in combination with GEMMA, a linear mixed model method which corrects for differences in relatedness among strains.[26] We mapped using a set of 20 kinship matrices, each computed by excluding all markers on one of the 19 autosomes or the X chromosome.[91] Support intervals are given by the –2.0 logP drop from the signal peak. Effect sizes are uncorrected for the Beavis effect but do not include parental phenotypes.[92–94] To ensure the reproducibility of our results, we have shared the detailed mapping protocol on protocols.io (dx.doi.org/10.17504/protocols.io.n92ld8pb7v5b/v1).

Mapping mRNA expression

We mapped every gene on the locus separately from the "UTHSC BXD Aged Hippocampus Affy Mouse Gene 1.0 ST(Sep 12) RMA Exon Level" dataset provided in GeneNetwork.org (GN Accession: GN392). In this process, we chose between multiple results per gene based on the number of represented strains overlapping with the PGB strains, standard error being low, effect sizes being high and the highest association scores. We noted the mean mRNA expression, given as a normalized Z-like score value with a mean value of eight units with a SD of two in the hippocampal array data, to confirm the gene was represented in our tissue of interest.[88] Values lower than seven were considered to represent negligible expression. *cis*-eQTLs using microarray data can contain false positives due to higher binding affinity of the B allele, for which the microarray probes were designed. We reduced the possibility of the *cis*-eQTL being a probe binding artifact by verifying its existence in other tissues, following the assumption that the *cis*-eQTL effect being predominantly conserved over tissues.[95] Furthermore, we have prioritized candidates without proven irregularities in array sets found in mismatched SNP alleles on the UCSC Genome Browser (RRID:SCR_005780; https://genome.ucsc.edu/)[84] for mouse genome (GRCm38/mm10), another redirection given by GeneNetwork.org to verify probes via the BLAT tool.[96] Although we cannot exclude the effects of all potential confounders that could affect covariance, we did rule out effects of sex, kinship and batch effects.

Identification of allele variations affecting protein function

Proteomics data on the BXD family provided by David Ashbrook were used to investigate predicted protein altering segregating variants and whether those would be predicted to be deleterious variants according to the Ensembl Variant Effect Predictor (RRID:SCR_007931), providing another category measuring the severity of consequences of gene variation in the family.[27,29] Subsequently, we examined genes with a high number of mutations based on Wang et al., 2016, which indicates the mutation severity based on the maximum Grantham score.[31]

Age associated gene expression changes

Age-associated gene expression changes were quantified using bulk RNA-seq data from C57BL/6J male mouse hippocampi across the lifespan (2 months, 12 months, 24 months, n=3 per timepoint) (Table S3).[28] Raw paired end sequencing reads were quality assessed and processed through fastp (v0.20.1; RRID:SCR_016962; Phred quality > 40; 10% unqualified bases permitted).[78] Processed reads were mapped and quantified using Salmon (v1.10.1; RRID:SCR_017036) in mapping-based mode with seqBias, gcBias and posBias parameters enabled.[81] A decoy-aware transcriptome assembly (concatenated genome and transcriptome) used for mapping was derived using *Mus musculus* GRCm38 reference files (release 102 from Ensembl). Gene level expression estimates were achieved using tximport (v1.22.0; RRID:SCR_016752) and normalized counts calculated using DESeq2 (v.1.34.0; RRID:SCR_015687).[76,83]

Assessing cell type specific expression

We used the Yao et al. (2023) scRNA-seq dataset to assess the cell-type specificity of the candidate genes.[32] The Jin et al. (2025) scRNA-seq dataset was then leveraged to validate their expression across distinct brain regions, and enabled a comparison of Smarcal1 and Usp37 expression between young and aged mice.[33] Finally, the Lee et al. (2022) scRNA-seq dataset enabled a comparison between APDAs and all other astrocytes.[15] UMAPs were plotted using the SCANPY python package.[82]

Contextual fear conditioning data collection

Studies have shown that conditioned fear memory (CFM) is an effective readout of hippocampal function in terms of spatial memory and learning confidence, and demonstrated readable outcomes in cognitive performance tests in an age-related context.[49–51,97,98] Contextual fear conditioning was performed as previously described.[47] This was used to characterize cognitive function across the B-BXDs at either 6 or 14 months of age. We used F1 crosses between the C57BL/6J and BXD strains (B6-BXDF1s), as these were being phenotyped in a parallel project. Specifically, we used 363 mice, both female and male, of 6-22 months old (GN trait ID: 5XF_10474, Table S3). On the first day of training, mice were placed in a training chamber and four 0.9 mA 1 s foot shocks were delivered after a baseline period of 180 s and then repeatedly after an interchangeable interval of 115 ± 20 s. Four post-shock intervals were defined as 40 s following the offset of each foot (Colbourn Instruments, PA, United States). The percentage of time spent freezing following the final shock was used as a measure of contextual fear acquisition across the panel. Twenty-four hours after training, mice were placed back into the training chamber and the percentage of time spent freezing throughout the entire 10-min test was measured as an index of contextual fear memory (Figure 5D). A DeepLabCut model was trained to recognize 13 points on a mouse, in accordance with the labelling system of Sturman et al., 2020.[75] DLCAnalyzer was used to measure freezing events.[75] For more information see Figures 5E–5G.

Y-maze data analysis

A Y-maze test in F1 crosses of BXDs and non-transgenic C57BL/6J was used to assess short-term spatial memory performances in a novel environment, including 276 mice in total, female and male (GN trait ID: 5XF_10013) (Table S3). Sessions were conducted over 10 minutes, during which the performance was recorded using a Raspberry Pi camera operating at 30 frames per second. Video frames were labeled and trained using DeepLabCut (RRID:SCR_021391) to track animals in the maze.[75,99] Alternation behavior was assessed using an R script integrated with DLCAnalyzer.[75] A mouse was counted to have entered an arm of the maze when the tail base crossed into that region. Mice exhibiting fewer than seven total alternations throughout the testing were excluded from further analysis. A correct alternation was recorded when a mouse exited one arm and subsequently entered a new arm, not last explored (Figure 5H). A percentage of incorrect and correct alternations was computed out of the recorded data on a single subject basis. For more information see Figures 5I–5K.

QUANTIFICATION AND STATISTICAL ANALYSIS

Protein structure prediction

Protein structure predictions of Smarcal1, Usp37, Zfp142, and Stk36 were performed using either the AlphaFold model on the web browser of Ensembl (release 112) (Figure 4D) or a local AlphaFold implementation (employing python v.3.10.13; hmmer suite v.3.4; hhsuite v.3.3.0; kalign v.3.4.0; ptxas v.11.7.64) (Figure 4E).[79,99] Calculations were executed on computer servers with AMD EPYC 7F52 16-core processors. Modeling was run using default options (e.g. full genetic database configuration) with five seeds for each of the five models. The AlphaFold confidence score was employed to rank the predictions, and the prediction with the highest score is shown.

Differential expression analysis in older BXD animals

To detect a possible relationship between PGB burden and cognition in aged hippocampus, a differential expression analysis was carried out between *Pgb1* DD and BB alleles in mice older than 600 days. To this end, transcriptome data from a total of 72 mice, 36 with DD and 36 with BB alleles were used (GN712). Only protein coding genes were kept for downstream analysis (n=15876). First, a linear model for every transcript of the expression matrix was created with the lmFit function from the limma R package, which performs for each gene a t-test in the case of a two-class comparison.[79] Then, statistical determination of differential expression (moderated t-statistics, moderated F-statistic, and log-odds) were computed by the empirical Bayes method through the eBayes function

from the same R package. DEGs were defined using a p-value threshold of 0.05 and represented in a volcano plot using ggplot2 R package (Figure 5A). To investigate whether the DEG list (with unadjusted p-values) was enriched for cognition associated genes, the intersections between the DEGs and two independent cognition related gene lists, the GO:0050890_cognition list with 249 genes and the MP:0014114_abnormal_cognition list with 1197 genes (Table S6), were tested through a Fisher's exact test using testGeneSet from the CoExpNets R package.[37,74,85] The p-value threshold for significant intersections was set at 0.05 (Figures 5B and 5C).

PGB burden impact on cognitive performance

To assess the potential influence of PGB accumulation in hippocampal astrocytes on learning and memory functions, a search was conducted using the dataset: ''UTHSC BXD Aged Hippocampus Affy Mouse Gene 1.0 ST (Sep12) RMA Exon Level'' (GN Accession: GN392) (137 animals, males and females of 11-25 months-old). The search was "rif=learning", where rif = reference into function—an NCBI summary of gene functions with links to references. The list of results was sorted by peak location and focused on the genes that map to 72–75 Mb (–log*P* values > 2.0). Finally, mapping was repeated using GEMMA to validate the results.

Phenome-wide association analysis of the *Pgb1* locus

Two SNP markers within *Pgb1* were selected: (1) a proximal marker, rs31200269, at 72.62 Mb and (2) a distal marker, rs13475923, at 74.07 Mb. These markers are in strong linkage (r^2 = 0.79) and only two strains among those phenotyped differ in their genotypes—BXD23 and BXD29. Both proximal and distal markers were used as proxies for the *Pgb1* locus and in the phenome-wide association analysis, using the full spectrum of BXD-datasets available on GeneNetwork.org, to find traits that both covary with these markers and that map within the *Pgb1* locus with linkage scores (–log*P* values > 2.0). Candidate phenotypes, including expression traits, were considered of high interest when they were associated with behavioral differences or with the metabolism of glycogen or the formation of other types of aggregates in the central nervous system. For more information see Tables 1 and 2.